Fault segmentation as constraint to the occurrence of the main shocks of the 2016 Central Italy seismic sequence

Pizzi A.[1], Di Domenica A.[1], Gallovič F.[2], Luzi L.[3], Puglia R.[3]

[1] University "G. d'Annunzio", Chieti-Pescara, Italy
[2] Charles University, Faculty of Math. and Physics, Dept. of Geophysics, Prague, Czech Republic
[3] Istituto Nazionale di Geofisica e Vulcanologia, Milano, Italy

Correspondence to:
pizzi@unich.it

Key points:

- Slip inversion and surface faulting show that fault segmentation and structural barriers controlled rupture propagation of the three main events
- The involved normal faults are breaching through existing relay zones as suggested by fault linkage models
- Soft-linkage between faults separated by transversal barrier may increase the maximum expected magnitude by the occurrence of single rupture

Keywords:
coseismic ruptures, slip inversion, structural barriers, fault segmentation, 2016 Central Italy seismic sequence, earthquake hazard

Abstract

We perform the finite-extent fault inversion of the three main events of the 2016 Central Italy seismic sequence using near-source strong-motion records. We demonstrate that both earthquakes nucleation and rupture propagation were controlled by segmentation of the (N)NW–(S)SE-trending Quaternary normal faults. The first shock of the sequence (August 24th, Mw 6.0) ruptured at the relay zone between the Laga Mts (LF) and the Cordone del Vettore (CVF) normal faults. The second shock (October 26th, Mw 5.9) nucleated at a minor relay zone within the Mt. Vettore–Mt. Bove fault (VBF), while the third and largest one (October 30th, Mw 6.5) initiated at the relay zone between the VBF and CVF, triggering the multiple rupture of the VBF, CVF and probably LF. We show that this latter relay zone corresponds to the deeper, high-angle, fault-zone of the Sibillini Mts cross-structure, a thrust-ramp inherited from the Miocene-Pliocene contractional phase of the Apennines. This structure acted as a barrier to rupture propagation of the first two events thus defining an area of large stress concentration until it acted as the initiator of the rupture originating the largest Mw 6.5 event that crossed the barrier itself. We suggest that the "young" CVF have started to cut through the barrier acting as a soft-linkage between the two long-lived LF and VBF. The evidence that coseismic cumulative slip shows a maximum at the CVF, provided by both slip inversion and original surface rupture data, suggests that the CVF is growing faster than the adjacent faults.

1. Introduction

Tectonically active areas are commonly characterized by fault alignments hundreds to thousands kilometers long. However, the ability to subdivide faults into individual seismogenic segments is crucial for seismic hazard assessments because it might permit to constrain the location of rupture initiation and termination, the length and the maximum expected magnitude of the seismogenic fault that will likely break during a single earthquake [*e.g.*, *Wells and Coppersmith*, 1994]. Several authors suggested that fault segment boundaries may correspond to peculiar geologic features such as major relay zones at faults step-over, pronounced bends or branch faults and large cross-faults [*e.g.*, *King and Nabelek*, 1985; *Crone et al*., 1991; *DePolo et al.*, 1991]. Many of these geologic features have therefore been interpreted as able to stop the propagation of coseismic ruptures and referred to as geometric and structural barriers [*Aki*, 1979]**.** From a mechanical point of view, barriers have been interpreted as zones of high fault strength, *i.e.*, more resistant to earthquake rupturing [*Aki*, 1979]; although experimental studies have suggested that also creeping weak seismic areas and compliant areas appear to be resistant to dynamic rupture [*Boatwright and Cocco, 1996*].

On the other hand, both theory and field observation show that the same geometric and structural barriers can act as points of rupture nucleation, also producing multisegment earthquakes, probably because they are zones of stress concentration [*Aki*, 1979; *King and Nabelek*, 1985; *Sibson*, 1986; *Boatwright and Cocco*, 1996; *Manighetti et al.*, 2015; *Perrin et al.*, 2016]. This dual behavior of the barrier, however, is not yet fully understood, although there are well-documented examples such as the 1983 Borah Peak earthquake [*Crone et al.*, 1987; *Aki*, 1989; *Susong et al.*, 1990].

This issue is also closely linked to another debated relevant question: could a large structural barrier, separating two approaching fault systems, remain persistent through time, at most only occasionally breaking during its history for particular conditions of dynamic stress and strain accumulation [*e.g., Schwartz and Coppersmith*, 1984; *King and Nabelek*, 1985; *Schwartz*, 1989; *Wesnousky*, 2008]? Or the barrier will eventually be by-passed by a newly formed fault that allows the progressive hard-linkage of the two approaching fault systems until a continuous throughgoing major structure forms [*e.g., Scholz and Gupta*, 2000; *Manighetti et al*., 2015; *DuRoss et al*., 2016; *Peacock et al.*, 2017]?

In this study, we examine the large geological and seismological dataset observed after the three main shocks of the 2016 Central Italy seismic sequence to address the above questions about the relation between earthquakes, fault segmentation and structural barriers.

Since August 2016, Central Italy was struck by one of the most important seismic sequences that ever took place in the country. The sequence is characterized by the occurrence of a series of shocks with increasing magnitude (Table 1; the reference Mw of this and other sequences after 2005 in central Italy are taken from the http://cnt.rm.ingv.it, whereas the Mw of the 1997-98 Umbria Marche sequence is from *Pondrelli et al.* [2002]): the first shock (Mw 6.0), which is identified as "Amatrice", occurred on August 24th at 01:32:36 UTC, a second large shock (Mw 5.9), identified as "Ussita", occurred on October 26th at 19:18:06 UTC and the third and largest (Mw 6.5), identified as "Norcia", occurred four days later, on October 30th 2016 at 06:40:18 UTC. The fault mechanism of the three shocks features pure normal faulting, with a NE–SW extension, in agreement with the predominant regime characterizing the Central Apennines. About 55,000 aftershocks have been recorded in five months following August 24th, 62 of them with moment magnitude in the range of 4-5.5.

The three main shocks of the sequence occurred in the axial zone of the Central–Northern Apennines affected by (N)NW–(S)SE active normal fault systems. Surface ruptures, seismicity distribution and satellite data (*e.g., Livio et al.* [2016] and references therein) largely agree upon the attribution of these events to the activation of at least two normal fault systems: the Mt. Vettore–Mt. Bove [*Calamita et al.*, 1992] and the Laga Mts [*e.g., Galadini and Galli*, 2000]. Each of these two fault systems extends for a length of ca. 25-30 km, occupying a sector of the chain characterized by the absence of historical seismicity so that they were considered as "silent" faults [*e.g., Galadini and Galli*, 2003]. On the other hand they show evidence of Late Pleistocene–Holocene activity [*e.g., Calamita et al.*, 1992; *Coltorti and Farabollini*, 1995; *Cello et al.*, 1997; *Galadini and Galli*, 2000; *Pizzi and Scisciani*, 2000] and *Boncio et al.* [2004] associated the 1639 AD earthquake to the Laga Mts fault system. The area struck by this sequence lies to the southeast of the 1997 Colfiorito (Mw 6.0) fault zone and extends as far as to the area struck by the 2009 L'Aquila (Mw 6.1) sequence to the south (Figure 1).

The study area is characterized by a complex structural framework deriving from the interaction between pre-existing (Miocene-Pliocene) contractional structures (*e.g.*, folds and thrusts due to the emplacement of the Apennine chain) and Quaternary extensional faults (due to post-orogenic collapse) [*e.g.*, *Calamita and Pizzi*, 1994; *Tavarnelli et al.*, 2004]. In particular, Figure 1 shows (N)NW–(S)SE-trending Quaternary normal faults oblique to NNE–SSW-trending thrust ramps. Some authors evidence how the evolution of Quaternary/active seismogenic faults may be controlled by the interaction with pre-existing structures. Already in the work of *Calamita and Pizzi* [1994] some Quaternary faults were considered detaching on the Sibillini Mts thrust, differing from others faults that displace it and which were interpreted by the authors as the active and seismogenic structures.*Chiaraluce et al.* [2005] examined the 1997 Colfiorito (Mw 6.0) sequence, attributing the nucleation of the main shock of the sequence to the intersection of normal faults and pre-existing compressional-transpressional structures. In this case the authors interpreted the crosscutting structures as lateral barriers to rupture propagation, which had constrained the normal fault size. Subsequently, *Pizzi and Galadini* [2009] discussed the role of pre-existing cross-structures (inherited from pre-Quaternary tectonic phases) on the propagation and segmentation of active Quaternary seismogenic extensional faults in the Central Apennines. They conclude that regional basement/crustal oblique pre-existing cross-structures, with lengths ranging from several tens of kilometers to hundreds kilometers (such as the NNE-striking Sibillini Mts thrust ramp), may act as "persistent structural barriers" that halt fault systems propagation, thus determining their terminations and maximum sizes. Regarding the 2016 Central Italy earthquakes, *Chiaraluce et al.* [2017] recognized the presence of barriers and asperities controlling the development of the seismic sequence. On the other hand, other authors disagree about pre-existing structures having an effect on earthquakes distribution and fault segmentation in central Italy [*e.g.*, *Roberts and Michetti*, 2004].

Therefore, it is important to further investigate the role of pre-existing structures because many studies outlined that the relationship between pre-existing thrusts and normal faults is of major importance for seismic hazard assessment. These relationships, indeed, may control rupture propagation in time and space, hence the rupture size and the related maximum earthquake magnitude as neighbour faults may rupture together generating earthquakes greater than those expected from the activation of a single fault segment [*e.g.*, *Pizzi and Galadini*, 2009 and references therein]. Most of these recent ideas have not yet been confirmed, and the 2016 seismic sequence represents a good choice to shed light on the relationships between active normal faults and pre-existing structural barriers.

In this work we invert the strong-motion records of the three main shocks of the sequence in order to obtain the slip distribution of each event, using the LinSlipInv method [*Gallovič et al.*, 2015]. We reconstruct the rupture episodes and relate the fault slip and aftershocks distribution to the main tectonic and stratigraphic features of the area, in order to explore whether the segmentation of normal faults and pre-existing compressional-transpressional structures may have conditioned the evolution of the sequence.

2. Geological setting

The Apennine chain is an Oligocene-Quaternary fold-and-thrust belt that developed following the convergence of the African and European continental margins [*e.g.*, *Boccaletti et al.*, 1990; *Carmignani and Kligfield*, 1990; *Doglioni*, 1991]. Its present-day structural framework derives from the succession of multiple extensional and contractional deformation events [*e.g.*, *Elter et al.*, 1975; *Castellarin et al.*, 1982; *Scisciani et al.*, 2002; *Tavarnelli et al.*, 2004; *Butler et al.*, 2006; *Calamita et al.*, 2011; *Di Domenica et al.*, 2012, 2014a, 2014b]. During the Neogene, the orogenesis affected Triassic-to-Miocene sedimentary successions related to different basin and platform domains of the Adria Mesozoic paleomargin [*e.g.*, *Ciarapica and Passeri*, 2002; *Patacca and Scandone*, 2007]. Successively, a Quaternary post-orogenic extension affected the axial sector of the Apennines developing (N)NW–(S)SE-trending normal fault systems, 15 to 35 km long, associated to intramontane basins and present-day seismicity [*e.g.*, *Calamita and Pizzi*, 1994; *Lavecchia et al.*, 1994; *Ghisetti and Vezzani*, 1999; *Galadini and Galli*, 2000]. Normal fault kinematics is fully consistent with the focal mechanism solution of the events located in the Central Apennines by instrumental seismicity [*Pondrelli et al.*, 2011].

The area struck by the Mw 6.5 Central Italy seismic sequence has an overall structural architecture dominated by a curve-shaped fold-and-thrust system, delimited to the east by the Miocene-Pliocene Sibillini Mts thrust (MST; Figure 1). The MST juxtaposes the Triassic–Miocene Umbria–Marche carbonate succession on to the Messinian siliciclastic turbidites of the Laga Formation. Parallel to the MST, the Mt. Cavallo thrust (MCT; Figure 1) changes its alignment in correspondence of Mt. Fema, within the Umbria–Marche succession. Along their NNE–SSW-trending arms, these features behaved as oblique thrust ramps and were characterized by transpressional kinematics [*e.g.*, *Calamita et al.*, 1987; *Calamita and Deiana*, 1988; *Tavarnelli et al.*, 2004]. Often they correspond with important lateral facies changes in the pre-orogenic stratigraphy, constituting long-lived fault zones reactivated as crustal-scale regional thrust ramps in Miocene-Pliocene time (*e.g.*, ancient Ancona–Anzio line separating the Umbria–Marche pelagic domain from the Lazio–Abruzzi platform domain, reactivated as the MST; *Castellarin et al.* [1982]). As already mentioned above, they are oblique to the Quaternary normal fault systems and may represent pre-existing structural barriers that compartmentalize active and seismogenic normal faults at depth, controlling their growth, development and associated seismicity [*e.g.*, *Pizzi and Galadini*, 2009; *Di Domenica et al.*, 2012]. Understanding the role of such geological-structural barriers is of primary importance to better define normal fault segmentation, with implication on the maximum expected magnitude and seismic hazard assessment.

In the area struck by the 2016 Central Italy seismic sequence two neighbouring normal fault systems are present: the Mt. Vettore–Mt. Bove [*Calamita et al.*, 1992] and the Laga Mts [*e.g.*, *Galadini and Galli*, 2000], respectively located in the hanging-wall and footwall of the MST (Figure 1). Although the August 24th and October 30th coseismic ruptures indicated the reactivation of both systems and crossed the MST trace [*e.g.*, *Livio et al.*, 2016] (Fig. 2), the MST may well have behaved as a structural barrier at depth, controlling the rupture termination of the August 24th event [*Chiaraluce et al.*, 2017] and the initiation of the third M 6.5 stronger event, as later discussed in the text. Moreover, individual fault segments within the Laga Mts and Mt. Vettore–Mt. Bove systems, with different lengths (5 to 15 km) and geologic throws (up to ca. one thousand of meters), can be still separated by rock volumes (more or less evident) referred to relay zones [*e.g.*, *Peacock and Sanderson*, 1994; *Childs et al.*, 1995] (Figure 2).

The Mt. Vettore–Mt. Bove structure was studied in detail for the first time by *Calamita et al.* [1992] and *Calamita and Pizzi* [1994] and was defined as an active normal fault system characterized by a total length of about 30 km limited, toward the north, by a progressive reduction of throws near the Ussita and Cupi villages area, while throws sharply decrease toward the south, approaching the oblique structural barrier of the Miocene-Pliocene MST whose trace could have been downthrown of about 100-200 m by the easternmost normal fault segment (Figures 1 and 2). The system is constituted of several NNW–SSE-trending kilometers long sub-parallel primary and secondary faults, both synthetic and antithetic, with oblique transfer fault segments, en-échelon patterns and relay zones. In the present work we will distinguish the Mt. Vettore–Mt. Bove fault system (VBF) from the south-easternmost segment, *i.e.*, the Cordone del Vettore fault, which is characterized by a very clear and continuous fault scarp (CVF; Figures 1 and 2). Within the VBF we further distinguish the northernmost Cupi segment (CF; Figure 2), activated during the October 26th event, based on coseismic ruptures mapped in the field, from the central–southern sector (Mt. Bove segment: BF; Figure 2). The CVF runs at ca. 2000 m of altitude along the Mt. Vettore western slope and was considered active by *Calamita et al.* [1992], while *Galadini and Galli* [2003] emphasized the recent activity of a normal fault affecting an alluvial fan in the Castelluccio basin. Here they recognized three paleoearthquakes, the youngest constrained between 4155-3965 years BP and the 6th-7th century A.D. This latter fault is probably a minor western splay of the major Mt. Vettore–Castelluccio basin boundary fault which shows a maximum cumulative geologic throws >1000 meters [*Pizzi et al.*, 2002] and represents the southernmost sector of the VBF.

In the MST footwall, the Laga Mts fault system (LF) extends from Accumoli to Campotosto with a NNE–SSW trend and with lengths comparable to the Mt. Vettore–Mt. Bove system (Figure 1). This system has been considered active by various authors [*Calamita and Pizzi*, 1994; *Cello et al.*, 1997; *Galadini and Galli*, 2000] and *Boncio et al.* [2004] associated the 1639 AD earthquake to this fault system. On the other hand, some studies stated that Late Pleistocene-Holocene activity can only be related to the southern portion of the system [*Galadini and Messina*, 2001] and *Galadini and Galli* [2003] recognized two displacement events after 8320-8150 years BP in this sector. The southern portion of the system has been probably partially activated during the 2009 L'Aquila seismic crisis [*Chiaraluce et al.*, 2017 and references therein]. The system shows cumulative geologic throws exceeding 2000 m and it is confined to the south by the Gran Sasso thrust and to the north by the MST (Figure 1), defining a stepover zone with the Mt. Vettore–Mt. Bove fault system [*Boncio et al.*, 2004].

3. Finite fault inversion

3.1 Data

A finite fault inversion for the three largest events of the 2016 Central Italy seismic sequence has been performed on the strong-motion data recorded by the Rete Accelerometrica Nazionale (RAN) and the Rete Sismometrica Nazionale (RSN), the former operated by the Italian Department of Civil Protection and the latter by the Istituto Nazionale di Geofisica e Vulcanologia. The records have been extracted from the Engineering Strong-Motion database [*Luzi et al.*, 2016a, 2016b], where about 10,000 strong-motion records are available for this sequence, all of them quality checked and manually processed. For the inversion of each event we have used all three-component strong-motion waveforms recorded by stations with a distance up to about 50 km from the fault.The number of stations ranges between 20 and 30 due to the fact that the Ussita and Norcia events were recorded by additional temporal stations deployed after the Amatrice earthquake. For the three major earthquakes there are several stations lying just above the Mt. Vettore–Mt. Bove and Laga Mts normal fault systems, providing exceptionally good resolution of the rupture process (Figure 3).

3.2 Method

Fault slip inversions were performed using the LinSlipInv method [*Gallovič et al.*, 2015; https://github.com/fgallovic/LinSlipInv]. Fixing fault geometry and rake angle, the fault is discretized to a relatively fine grid of sub-faults of approximately 1x1 km. Each sub-fault is associated with sought general slip rate function, discretized in time, covering the whole duration of the rupture process. The spatial-temporal samples of the slip rates represent the model parameters of the inverse problem. To regularize the solution, we consider a *k*-squared prior covariance function and constrain the event seismic moment [*Gallovič et al.*, 2015]. Furthermore, we seek for positive values of the slip rates (no back-slip) by means of using the non-negative least-squares approach by *Lawson and Hanson* [1974]. This way, the method considers a general rupture parameterization, with no a priori constraints on the position of the nucleation point, rupture speed, and shape of slip-rate functions. Thus, it is able to retrieve even a complex style of rupture propagation. However, as in any multiparameter inversion, the rupture model is sensitive to artifacts and biases imposed by the smoothing constraint and imperfect modeling of the general 3D velocity structure, as analyzed in detail by *Gallovič et al.* [2015]. They found that *i*) the slip rate functions are smeared in time and space due to the smoothing constraint, *ii*) the time of the slip-rate maximum is the least biased source parameter, *iii*) imprecise Green's functions can introduce artificial slip-rate multiples, especially at shallow depths, which appear as "ghost" features in the rupture propagation (slip rate snapshots). Therefore, care must be taken when interpreting the inferred rupture images.

In all the cases the data and synthetics are filtered by a 4^{th} order causal Butterworth filter between 0.05 and 0.50 Hz (with one exception of station RQT in case of the Amatrice event where range of 0.1-0.5Hz was used). The waveforms were downsampled to the time step of 0.4 s. In order to strengthen the role of stations located further away from the fault, we increase their weight by a factor of 2 with respect to stations located above the fault. Synthetic Green's functions were calculated by the discrete wave number and matrix methods [*Bouchon*, 1981; *Coutant*, 1989; *Kennett and Kerry*, 1979] for a 1-D velocity model adopted from *Gallovič and Zahradník* [2012] and *Ameri et al.* [2012], for the low-frequency and broad-band modeling of the 2009 L'Aquila earthquake, respectively. We fix the parameter controlling the smoothing strength [*Gallovič et al.*, 2015] at a value providing a good balance between rupture complexity (minimum "ghost" features) and data fit and adopt this value for the three events. Furthermore, for each event we have performed a grid search over fault plane location, fault geometry (strike and dip), and slip direction (rake): the finite-faults slip inversion was repeated for each set of the grid-searched parameters. Model with the best (optimized) waveform fit has been selected as the preferred one.

3.3 Results

The fault geometries and location of the centroids are shown in Table 2. The seismic moments resulting from the inversion of the first two events are larger than the ones calculated by INGV, and used as reference in this paper (Table 1), but are in agreement with the values provided by Harvard Global CMT (http://www.globalcmt.org/). The waveform comparison between the observed and synthetic data for the final rupture models are shown in the electronic supplement (Figure 1S). In space the inferred (planar) faults of the three events align well in the along-strike direction, resembling a geometrically relatively simple normal fault (Figure 3). However, the inferred source models differ substantially in the style of rupture propagation and slip distribution.

In particular, the Amatrice event exhibits bilateral rupture propagation (Figure 4a), where the final slip consists of two overlapping circular-like slip patches (Figures 3a and 7a). A similar bilateral rupture was obtained by *Tinti et al.* [2016], but with well separated and smaller slip patches. This difference can be attributed to the regularization constraints applied by the two methods.

The Ussita earthquake is characterized by relatively simple unilateral rupture propagation towards NW (Figure 4b). These two events have maximum slip of 0.5 m and peak slip rates of approximately 0.3 m/s with rupture speed roughly 3 km/s.

The largest Norcia event has remarkably different style of rupture evolution (Figure 4c). Initially rupture propagates mainly updip and continues developing for 5-6 seconds. Due to the smoothing constraint we cannot decide whether this is due to very long rise time and/or very slow rupture propagation, or both. The peak slip rate reaches 1.2 m/s whereas the final slip is ~3 m. The rupture seems to continue SE from the nucleation, at shallow depth along strike, at a rupture speed of ~3 km/s. As the smoothing constraint generally makes the maximum amplitudes of slip and slip rates smaller than the true values, one can still compare the maxima of the three events, because the smoothing strength is the same in all the cases.

The obtained slip models are superimposed on the aftershocks distribution (from *Chiaraluce et al.* [2017]) and the main tectonic features of the area, in order to explain the relationship between the pre-existing geological structures and the rupture processes of the three events. In particular, the Sibillini Mts thrust ramp has been projected on the slip model providing fundamental key-points in the interpretation of the temporal and spatial evolution of the sequence (thick dashed line in Figure 4). The MST geometry has been defined following geological-structural constraints (see the discussion section) and seems to coincide with the zone where seismicity concentrated after the August 24th earthquake. The Amatrice event involved the footwall block of the MST and the rupture was stopped against the MST fault zone (Figure 4a). Similarly, the Ussita event occurred and propagated entirely in the hanging-wall block of the MST (Figure 4b). The Norcia event nucleated in correspondence of the fault intersection with the MST. Starting from this point, rupture propagated first upward and northward, *e.g.*, in the MST hanging-wall in a zone remained almost unruptured after the first two main shocks. Successively, the rupture by-passed the MST fault zone affecting the area in its footwall already involved during the Amatrice event (Figure 4c). These observations highlight that the MST acted as a barrier from the very beginning, determining the activation of single fault segments, delimiting the rupture length of the first two main shocks and localizing the stress in the MST fault zone itself.

4. Towards a 2D+ visualization of the geological volume involved in the sequence

The results of our inversion analysis provides a good tool to observe ruptures propagation in space and time and their geometric relations with the MST pre-existing mechanical barrier. Although for the slip inversions very simplified (planar) rupture planes are sufficient to fit the low-frequency observed data in spite of the high geological-structural complexities characterizing the study area, we tried to construct a more realistic 2D+ model based on a set of geological cross-sections. Because the fault systems are composed of sets of subparallel synthetic, antithetic, en-échelon Quaternary/active normal faults, oblique to pre-existing thrust faults, we have drawn five cross-sections, both perpendicular and parallel to the mean normal faults strike, all of them intersecting the epicenters of the five events with magnitudes larger than 5 (Figures 1, 5, 6 and 7).

The cross-sections have been constructed integrating the available surface and subsurface data in order to investigate possible relationships at depth among the geological-structural features, the ruptures evolution and the seismicity distribution. In particular, shallow geological boundaries and the pattern of Quaternary/active normal faults have been traced following the available geological and structural maps of the area [*e.g.*, *Servizio Geologico d'Italia*, 1941; *Calamita et al.*, 1992; *Pierantoni et al.*, 2013]. Considering the regional scale of the cross-sections, they have been simplified (*e.g.*, secondary thrusts and folds and pre-Quaternary faults have not been represented) highlighting the relationships between the active normal faults involved in the 2016 seismic sequence and the MST. Regarding subsurface stratigraphy, the "Varoni 001" well (available at http://unmig.sviluppoeconomico.gov.it/videpi/videpi.asp), which was drilled throughout the sedimentary succession for 5766 m, reaching the Triassic evaporites and dolostones, allowed us to better constrain the geological model in the MST footwall block. The geometry at depth of the MST has been defined, for the first 2-3 km, by field data which clearly show the low-angle dip of the thrust plane. At major depth this feature represents a high-angle oblique thrust ramp that reactivated a pre-existing normal fault (*e.g.*, Ancona-Anzio line; *Castellarin et al.* [1982]). The high-angle geometry of the thrust ramp is supported by geologic and seismic reflection data [*e.g., Tavarnelli et al.*, 2004; *Finetti et al.*, 2005] and has been drawn also considering the aftershocks distribution and the interpolation between all the sections. At 6-8 km of depth, the aftershocks distribution evidences a band characterized by scarce seismicity that we interpreted as a mechanically weak horizon ("detachment level" in Figure 7). This ~1.5 km thick band falls between the overlying drilled Triassic rocks, characterized by a relatively high seismicity, and an underlying zone with very high seismicity. According to the deep stratigraphy imaged by seismic reflection data available for areas more to the north [*Scisciani et al.*, 2014], this horizon can be referred to as a "detachment layer", attributed to the (?Upper) Paleozoic–(?Lower) Triassic sequence. In this view we assume that the zone underlying this layer, where seismicity concentrates, corresponds to a stronger rheological level (*e.g.*, the crystalline basement) where the Amatrice Mw 6.0 event seems to be nucleated. The other 5<Mw<6.5 events are located above the weak horizon, nucleating within the relative stronger Triassic sequence. At greater depths seismicity stops around 10-12 km, suggesting this level to be the upper boundary of the brittle-ductile transition that deepens towards the east (Figure 6). Such depth is in agreement with the rheological model of *Boncio et al.* [2004] proposed for the Norcia–Mt. Vettore area.

The comparison between fault patterns (including the 2016 coseismic ruptures and long-term geologic fault traces) and slip distribution (obtained by the inversion of the strong-motion data) has been used to reconstruct an "enhanced 2D" evolution of the main events. Clearly, this method suffers from limitations and assumptions: if on one hand the coseismic surface ruptures indicate a very complex pattern with primary and secondary rupture planes, the slip model, that we transposed on vertical cross-sections, indicates that the rupture apparently does not reach the topographic surface, as it is simplified to a single fault plane and constraints on the geometry of faults at depth are lacking. Nevertheless, the obtained results seem to be sufficiently robust as they have been obtained comparing independent data and methods.

Concerning the Amatrice Mw 6.0 event, slip inversion analysis shows that almost the whole slip occurred in the footwall block of the MST with a maximum value of 40-50 cm at a depth of 1 to 5 km (with respect to sea level) and a rupture length of 25-30 km (Figures 7a and 8). The hypocenter location and slip distribution also indicate that the rupture began in the footwall of LF, along the probable southern prosecution of the CVF, in correspondence to the overlapping area between the LF northernmost sector and the CVF southernmost sector (Figure 2 and section 1 of Figure 6). As already shown in Figure 4a, the slip model indicates that the rupture firstly proceeded toward the southeast and, after ca. 2-3 seconds, propagated toward the northwest. This pattern, therefore, may suggest different scenarios: *i*) the rupture could be started directly on the CVF or *ii*) the rupture started at the relay zone between two faults (Figure 2), activating first the LF and then the CVF. The latter case implies a complex rupture, suggesting that the two faults currently kinematically interact (soft-linkage) or are already linked (as also suggested by *Lavecchia et al.* [2016]). It is noteworthy that the northward propagation of the slip along the CVF was (almost completely) halted at the high-angle deeper part of the MST (Figure 7a and b; see also Figure 4a), which hence acted as a mechanical structural barrier [*sensu Pizzi and Galadini*, 2009; *Di Domenica et al.*, 2012], although the very shallow low-angle part of the MST was clearly displaced by the CVF (section 2 of Figure 6 and Figure 9). These geometric relationships are strongly supported by the surface rupture pattern following the August 24th earthquake, which showed the reactivation of the CVF, through the MST trace, for a surface length of about 5-6 km, starting ca. 2 km north of the Arquata del Tronto village up to the northernmost sector of the Mt. Vettore, with a maximum throw of ca. 20 cm (Figure 10). Conversely, the master fault segments of the VBF did not show evidence for reactivation, at least by surface rupture data. Surface rupture data therefore have a good accordance with those of the slip model, especially about rupture location and sites where the slip has reached the maximum values (Figure 7a), except in Accumoli-Amatrice southern area where the evidence for surface rupture is discontinuous and throw is not comparable with that observed along the CVF. We suggest that this latter inconsistency can be due to the different style of deformation associated with highly porous Messinian sandstones (Laga Formation) at the MST footwall, which usually develop wide cataclastic zone and are also decoupled from the underlying Tertiary-Mesozoic carbonate sequence by an interposed marly detachment level of Miocene age.

From August 24th to October 25th, the aftershocks distribution delineates minor breaks to the east of the Cordone del Vettore normal fault and a NE-dipping structure that may be interpreted as the antithetic fault of the Mt. Vettore (section 2 of Figure 6). Moreover, seismicity concentrated in proximity of the MST fault zone (Figures 4 and 7) as also visible in map view where aftershocks define a NNE–SSW-trending cluster parallel to the MST, likely corresponding to the structural barrier (*i.e.*, MST fault zone) at depth (see aftershocks distribution of the August 24th-October 25th period in Figure 5).

The slip inversion analysis of the Ussita Mw 5.9 event indicates that the whole slip occurred in the hanging-wall block of the MST with a maximum rupture length of ~25-28 km, at a depth of about 2-4 km with respect to sea level (Figures 7b and 8). Surface rupture mapping carried out soon after the Ussita event and before the Norcia event showed the reactivation at surface of the northernmost segment of the VBF (Cupi fault segment: CF, see Figure 2), with a maximum measured throw of 15-20 cm observed in the central sector of the CF (Figure 11) which corresponds with the area of maximum slip expected at surface by the inversion model (Figure 7b). This second relevant shock nucleated at a minor relay zone within the VBF (between the Mt. Bove and Cupi fault segments; Figure 2) and ruptured toward the northwest (Figures 4 and 7). It is to note that the overall seismicity related to this event (the northernmost of the 2016 sequence) is limited to the north by the Mt. Cavallo thrust (MCT in Figure 7), which hence assumes the role of a preexisting structural barrier similar to the parallel, and more to the south, MST. The fact that the 1997 Umbria-Marche seismic sequence was, similarly, limited to the south by the same structure (see Figure 1) also support this hypothesis.

Slip distribution of the first two main events highlights a slip gap in the central-southern sector of the VBF (Figures 7b and 8), where seismicity concentrated after August 24th (Figures 6 and 7). The gap was "filled" by the zone of maximum slip during the Norcia event, when the hypocenter localized just in correspondence of the MST structural barrier, in an area that remained almost unruptured after the August 24th and October 26th events, as clearly visible looking at the evolution of the slip distribution in time along section 3 (Figure 6) and section 5 (Figure 7). The area where the October 30th event nucleated, moreover, corresponds to the relay zone between VBF and CVF (Figure 2). The comparison among the slip propagation, already mapped geological structures and coseismic surface ruptures suggests that the first rupture occurred in the central-southern portion of the VBF (Mt. Bove fault segment, in correspondence of the Mt. Porche area; Figure 2) affecting the hanging-wall of the MST structural barrier. Slip seems propagating firstly toward the northwest (Figures 4c and 7), probably overlapping to the October 26th rupture zone, then toward the southeast, up to the Castelluccio basin, where surface rupture data indicate the reactivation of already mapped several minor synthetic and antithetic planes. The slip is subsequently transferred to the south (overstep) reactivating the Cordone del Vettore fault, where the maximum surface rupture of the entire area (1 to 2 meters) has been observed (Figure 10). In this way deformation overcame the MST barrier and propagated also in its footwall for many kilometers, probably activating part of the Laga Mts fault, as likely happened on August 24th. This suggests that not all the elastic deformation accumulated by the Cordone del Vettore fault was released on August 24th as the fault was still locked to the north by the MST barrier. On October 30th all the deformation has been accommodated. In this context, therefore, the Cordone del Vettore fault constitutes a by-pass that works as a zone of linkage between the Mt. Bove–Mt. Vettore, to the north, and the Laga Mts, to the south, fault systems (Figures 9 and 12).

Comparison between field observations and inversion results showed that much of the maximum rupture length and a percentage of at least 50% of the maximum slip evaluated by the inversion model for very shallow depth (2-4 km) have been "transferred" up to the surface. For the Amatrice and Ussita events, indeed, the sites of maximum slip at depth (*i.e.*, 30-50 cm) correspond, with good approximation, to the sites of maximum throw at surface (*i.e.*, 15-20 cm), whereas a slip ≥ 3 m at 2 km of depth produced 1-2 m of throw at surface. Moreover, these values highlight that there was a difference of about one order of magnitude between the slip produced by the two near M 6.0 earthquakes (*i.e.*, Amatrice and Ussita) with respect to that of M 6.5, both at depth and at surface. The fact that the slip obtained from the model usually does not reach the topographic surface (Figure 7), can be attributed to a limitation of the theoretical model or to the possibility that a considerable increasing of throw occurred at surface due to post-seismic afterslip. Field observation of fault ruptures, also within the 24 hours from the event and in some instances repeated in time, however, suggests that negligible afterslip occurred at least after one day from the quake and during the next 1-2 weeks along the CF and CVF. The strong match resulting between the ruptures location at depth and at surface, as well as between the maximum slip at depth and at surface (Figure 7), for lengths of kilometers to tens of kilometers and along highly variable topography, clearly indicates that most of the ruptures observed at surface are coseismic slip and not shaking-induced landslides.

5. Discussion and conclusions

The peculiar location, size and evolution of the ruptures related to the three main shocks of the 2016 Central Italy seismic sequence and the great quantity of geologic, geodetic and seismological data provides a unique opportunity to better understand the relation between earthquakes, fault segmentation and structural barriers. Here in particular we focused on the first-order structural barrier represented by the MST cross structure interposed between the VBF and LF nearby fault systems, as well as secondary barriers here defined as the intersegment zones along the same fault system. In general, our results seem to confirm the dual role exerted by barriers that act not only as obstacle to the rupture propagation, but can also concentrate stress and localize the rupture causing twin earthquakes [*Aki*, 1979]. While according to *Mildon et al.* [2017] strike-variable fault geometries are able to generate stress heterogeneities that control the distribution and limits of the ruptures, we observe that the August 24th and October 26th events demonstrate that the MST first acted as a barrier delimiting the two ruptures and subsequently begun to act as a stress concentrator. Following the high stress concentration in correspondence of the barrier itself, this latter then acted as an initiator of the rupture allowing the contemporaneous multiple rupture of the VBF, CVF and probably of the LF northernmost portion during the October 30th M6.5 event. This reconstruction is supported by the complex evolution of the sequence that showed an increasing seismicity with time. It is to note that such energy *vs* time pattern of the sequence – *i.e.*, events of magnitude from about 6 up to 7, close in time (*e.g.*, days-months) – is not a unique case in the Central Italy seismic history. It is sufficient to consider the 1997 Umbria-Marche sequence, where a M 5.7 event triggered 9 h later an adjacent M 6.0 event, which ruptured the same fault system farther to the north and the 1703 Norcia-L'Aquila sequences with two ca. M 6.7 events occurred on 19 January and 2 February [*Blumetti et al.*, 1995; *Chiaraluce et al.*, 2005; *Rovida et al.*, 2011]. Also paleoseismological studies based on 36Cl concentration indicate that the Holocene activity of the Fucino fault system, located just to the south with respect to the analysed fault systems (Lazio-Abruzzo region), experienced periods of multiple, clustered earthquakes [*Benedetti et al.*, 2013; *Cowie et al*., 2017]. Furthermore, the increasing cases worldwide that document clustering of strong events suggest that earthquake synchronization can be a common behaviour for seismogenic fault systems [*e.g.*, *Scholz*, 2010; *Sokos et al.*, 2016]. This evidence clearly implies that faults can "communicate" to each other [see discussion in *Benedetti et al.*, 2013]. We suggest that one of the possible mechanisms that allow faults to communicate and interact is exactly the presence of barriers. This is not really a contradiction because, as discussed before, a transversal structural barrier can constitute, since the beginning, a zone of rapid stress and strain accumulation due to the dynamic stress transferred by the activated nearby parallel fault system (*e.g.*, the VBF and the LF for the 2016 sequence?) up to reach the strain threshold triggering another large earthquake. Alternatively, it may be that the inherited MST fault zone endure as a persistent barrier to rupture over many earthquake cycles as the structural maturity of the fault increases, as suggested by the *DuRoss et al.* [2016] for the Tre Monti fault (Fucino fault system), and only later became a zone of rupture nucleation with the development of a new bypass fault. Based on the long term geological and morphotectonic evidence we take more for this last hypothesis.

The evolution of the study area can be schematized considering two growing normal fault systems (*e.g.*, the LF and VBF), which have started to kinematically interact, separated by a pre-existing oblique structural barrier (*e.g.*, the MST fault zone; Figures 9 and 12). In this model the two adjacent faults have grown separately during the Quaternary (Figures 12a and b), accumulating lengths of ca. 30 km and geologic throws larger than 1000 meters, with Late-Quaternary slip rates in the order of 0.5-0.6 mm/yr [*e.g.*, *Barchi et al.*, 2000; *Pizzi et al.*, 2002]. Successively, the stress and strain fields surrounding the two fault systems have probably started to interfere. According to *Duffy et al.* [2015] and *Peacock et al.* [2017 and references therein] such fault interaction produces areas of local stress concentration and perturbation that can cause the formation of secondary structures – *e.g.*, the CVF (Figure 12b). In this view, the "young" CVF cannot be really considered as an eastern splay of the VBF, as it would appear from the plan view (Figure 2), but rather an "independent" fault which has started in the footwall of the MST [*Calamita and Pizzi,* 1994] as an attempt of linkage between the LF and VBF. In particular, we suggest that the CVF is growing toward the north developing a soft-linkage with the VBF. This hypothesis seems to be supported by the fact that the highest throws during the two major events, both at depth (slip inversion model; Figures 6, 7 and 8) and surface (coseismic ruptures; Figure 10), have been recorded on the CVF, according to the fault linkage model which illustrates that the zone of linkage between two master faults is that where the major slip is accumulated and therefore is growing faster than the adjacent faults [*e.g.*, *Peacock and Sanderson*, 1994; *Childs et al.*, 1995]. This would also explain why the CVF is characterized by greater morphotectonic evidence, i.e., well-exposed and continuous fault plane, despite its cumulative geological downthrown being about an order of magnitude less than that of LF and VBF. In our model, slip data indicate that the LF probably activated together with the CVF both on August 24th and October 30th, suggesting that also these two normal faults are probably soft-linked at present. The January 18th, 2017 sequence, with the four Mw ≥ 5 events, not considered in this paper, also supports the activation of the central-northernmost sector of the LF.

In addition, the fact that the slip of the first two main shocks (August 24th and October 26th) has been essentially confined by the MST and that even the major event (October 30th) localized exactly on the deep MST fault zone, means that this latter still represents a structural barrier with respect to the VBF and CVF which are not yet in direct physical contact (*e.g.*, soft-linkage).

Probably in the future the CVF is likely to breach out the sector of the barrier that will remain as an irregularity on the new through-going continuous fault surface (*e.g.*, hard-link between VBF and CVF and, possibly, LF), and both the asperity and the continuous fault may be by-passed at a later stage (Figure 12c). This evolution model has implication on the seismic hazard of the area as single faults 10–15 km long might be capable of generating M 5.5-6.0 earthquakes, while the breaching of the barrier might be associated to M 6.5 events or larger, as occurred during the 2016 seismic sequence. We believe, however, that our understanding of fault interaction at relay zones and across structural barriers must be improved through multidisciplinary studies regarding field geology, paleoseismology, geophysics, stress transfer modeling, etc. also considering the implications for seismic hazard assessment in Italy and worldwide.

Acknowledgments

We greatly thank Gerald Roberts and an anonymous reviewer for their constructive reviews and the Associate Editor Claudio Faccenna for his helpful comments.We thank Lauro Chiaraluce and his co-workers for making available the relocated aftershocks of the sequence before the public release. Slip inversions are performed using the LinSlipInv method [*Gallovič et al.*, 2015; https://github.com/fgallovic/LinSlipInv]. Geological and structural data supporting our conclusions are listed in the references. This work was funded by the Italian Ministry for Education, University and Research (MIUR) (ex 60% grants to A. Pizzi). Supporting information include three figures showing the comparison between observed and simulated waveforms for the three main events of the 2016 Central Italy seismic sequence.

References

Aki, K. (1979), Characterization of barriers on an earthquake fault, *J. Geophys. Res.*, 84, B11, 6140-6148.

Aki, K. (1989), Geometric features of a fault zone related to the nucleation and termination of an earthquake rupture, U.S. Geol. Surv. Open File Rep., 89–315, 1–9.

Ameri, G., F. Gallovic, and F. Pacor (2012), Complexity of the Mw 6.3 2009 L'Aquila (Central Italy) earthquake: 2. Broadband strong-motion modeling, *J. Geophys. Res.*, 117, B04308, doi:10.1029/2011JB008729.

Barchi, M., F. Galadini, G. Lavecchia, P. Messina, A. M. Michetti, L. Peruzza, A. Pizzi, E. Tondi, and E. Vittori (2000), *Sintesi delle conoscenze sulle faglie attive in Italia Centrale: parametrizzazione ai fini della caratterizzazione della pericolosità sismica*, CNR-Gruppo Nazionale per la Difesa dai Terremoti, Roma.

Benedetti, L., I. Manighetti, Y. Gaudemer, R. Finkel, J. Malavieille, K. Pou, M. Arnold, G. Aumaitre, D. Bourles, and K. Keddadouche (2013), Earthquake synchrony and clustering on Fucino faults (Central Italy) as revealed from in situ ^{36}Cl exposure dating, *J. Geophys. Res. Solid Earth*, 118, 4948–4974, doi:10.1002/jgrb.50299.

Blumetti, A.M. (1995), Neotectonic investigations and evidence of paleoseismicity in the epicentral area of the January–February 1703, Central Italy, earthquakes, L. Serva (Ed.), Perspectives in paleoseismology, *Association of Engineering Geologist*, Special Publication, 6, 83-100.

Boatwright, J., and M. Cocco (1996), Frictional constraints on crustal faulting, *J. Geophys. Res*., 101, 13,895–13,909, doi:10.1029/96JB00405.

Boccaletti, M., F. Calamita, G. Deiana, R. Gelati, F. Massari, G. Moratti, and F. Ricci Lucchi (1990), Migrating foredeep-thrust belt systems in the northern Apennines and southern Alps, *Palaeogeogr., Palaeoclimatol., Palaeoecol.*, 77, 41–50, doi:10.1016/0031-0182(90)90095-O.

Boncio, P., G. Lavecchia, and B. Pace (2004), Defining a model of 3D seismogenic sources for Seismic Hazard Assessment applications: the case of central Apennines (Italy), *J. Seismol.*, 8, 407–425, doi:10.1023/B:JOSE.0000038449.78801.05.

Bouchon, M. (1981), A simple method to calculate Green's functions for elastic layered media, *Bull. Seism. Soc. Am.*, 71, 959–971.

Butler, R. W. H., E. Tavarnelli, and M. Grasso (2006), Structural inheritance in mountain belts: an Alpine-Apennine perspective, *J. Struct. Geol.*, 28, 1893–1908, doi:10.1016/j.jsg.2006.09.006.

Calamita, F., and G. Deiana (1988), The arcuate shape of the Umbria-Marche-Sabina Apennines (Central Italy), *Tectonophysics*, 146, 139–147, doi:10.1016/0040-1951(88)90087-X.

Calamita, F., G. Deiana, C. Invernizzi, and S. Mastrovincenzo (1987), Analisi strutturale della "linea Ancona-Anzio Auctorum" tra Cittareale e Micigliano (Rieti), *Boll. Soc. Geol. It.*, 106, 365–375.

Calamita, F., and A. Pizzi (1994), Recent and active extensional tectonics in the southern umbro-marchean Apennines (central Italy), *Mem. Soc. Geol. It.*, 48, 541–548.

Calamita, F., A. Pizzi, and M. Roscioni (1992), I "fasci" di faglie recenti ed attive di M. Vettore–M. Bove e di M. Castello–M. Cardosa (Appennino Umbro–Marchigiano), *Studi Geologici Camerti*, spec. vol. 1, 81–95, available on-line at researchgate.net.

Calamita, F., S. Satolli, V. Scisciani, P. Esestime, and P. Pace (2011), Contrasting styles of fault reactivation in curved orogenic belts: Examples from the Central Apennines (Italy), *Geol. Soc. Am. Bull.*, 123, 1097–1111, doi:10.1130/B30276.1.

Carmignani, L., and R. Kligfield (1990), Crustal extension in the northern Apennines: the transition from compression to extension in the Alpi Apuane Core-Complex, *Tectonics*, 9, 1275–1303, doi:10.1029/TC009i006p01275.

Castellarin, A., R. Colacicchi, A. Praturlon, and C. Cantelli (1982), The Jurassic-Lower Pliocene history of the Ancona-Anzio line (Central Italy), *Mem. Soc. Geol. It.*, 24, 325–336.

Cello, G., S. Mazzoli, E. Tondi, and E. Turco (1997), Active tectonics in the central Apennines and possible implications for seismic hazard analysis in peninsular Italy, *Tectonophysics*, 272, 43–68, doi:10.1016/S0040-1951(96)00275-2.

Chiaraluce, L., M. Barchi, C. Collettini, F. Mirabella, and S. Pucci (2005), Connecting seismically active normal faults with Quaternary geological structures in a complex extensional environment: the Colfiorito 1997 case history (northern Apennines, Italy), *Tectonics*, 24, TC1002, doi:10.1029/2004TC001627.

Chiaraluce, L., R. Di Stefano, E. Tinti, L. Scognamiglio, M. Michele, E. Casarotti, M. Cattaneo, P. De Gori, C. Chiarabba, G. Monachesi, A. Lombardi, L. Valoroso, D. Latorre, and S. Marzorati (2017), The 2016 Central Italy Seismic Sequence: A First Look at the Mainshocks, Aftershocks, and Source Models, *Seismol. Res. Lett.*, 88(3), doi:10.1785/0220160221.

Childs, C., J. Watterson, and J. J. Walsh (1995), Fault overlap zones within developing normal fault systems, *J. Geol. Soc. London*, 152, 535–549.

Ciarapica, G., and L. S. Passeri (2002), The paleogeographic duplicity of the Apennines, *Boll. Soc. Geol. It.*, spec. vol. 1, 67–75.

Crone, A.J., and K.M. Haller (1991), Segmentation and the coseismic behavior of Basin and Range normal faults: examples from east-central Idaho and southwestern Montana, U.S.A., *J. Struct. Geol*., 13(2), 151-164.

Crone, A.J., M.N. Machette, M.G. Bonilla, J.J. Lienkaemper, K.L. Pierce, W.E. Scott, and R.C. Bucknam (1987), Surface faulting accompanying the Borah Peak earthquake and segmentation of the Lost River fault, central Idaho, *B. Seismol. Soc. Am*., 77(3), 739-770.

Coltorti, M., and P. Farabollini (1995), Quaternary evolution of the Castelluccio di Norcia basin (Umbro-Marchean Apennines, central Italy), *Il Quaternario*, 8, 149–166.

Coutant, O. (1989), *Program of numerical simulation AXITRA*, Tech. rep., Lab. de Geophys, Interne et Tectonophysics, Grenoble, France.

Cowie P.A., R.J. Phillips, G.P. Roberts, K. McCaffrey, L.J.J. Zijerveld, L.C. Gregory, J. Faure Walker, L.N.J. Wedmore, T.J. Dunai, S.A. Binnie, S.P.H.T. Freeman, K. Wilcken, R.P. Shanks, R.S. Huismans, I. Papanikolaou, A.M. Michetti, and M. Wilkinson (2017), Orogen-scale uplift in the central Italian Apennines drives episodic behaviour of earthquake faults, *Scientific Reports*, 7, 44858, doi:10.1038/srep44858.

DePolo, C. M., D.G. C lark, D.B. Slemmons, and A.R. Ramelli (1991), Historical surface faulting in the Basin and Range province, western North America: implications for fault segmentation, *J. Struct. Geol.*, 13(2), 123-136.

Di Domenica, A., L. Bonini, F. Calamita, G. Toscani, C. Galuppo, and S. Seno (2014a), Analogue modeling of positive inversion tectonics along differently oriented pre-thrusting normal faults: an application to the Central-Northern Apennines of Italy, *Geol. Soc. Am. Bull.*, 126(7-8), 943–955, doi:10.1130/B31001.1.

Di Domenica, A., P. Petricca, F. Trippetta, E. Carminati, and F. Calamita, F. (2014b), Investigating fault reactivation during multiple tectonic inversions through mechanical and numerical modeling: an application to the Central Apennines of Italy, *J. Struct. Geol.*, 67, 167–185, doi:10.1016/j.jsg.2014.07.018.

Di Domenica, A., A. Turtù, S. Satolli, and F. Calamita (2012), Relationships between thrusts and normal faults in curved belts: new insight in the inversion tectonics of the Central-Northern Apennines (Italy), *J. Struct. Geol.*, 42, 104–117, doi:10.1016/j.jsg.2012.06.008.

Doglioni, C. (1991), A proposal of kinematic modelling for W-dipping subductions – possible applications to the Tyrrhenian-Apennines system, *Terra Nova*, 3, 423–434, doi:10.1111/j.1365-3121.1991.tb00172.x.

DuRoss, C.B., S.F. Personius, A.J. Crone, S.S. Olig, M.D. Hylland, W.R. Lund, and D.P. Schwartz (2016), Fault segmentation: New concepts from the Wasatch fault zone, Utah, USA, *J. Geophys. Res. Solid Earth*, 121, 1131-1157, doi:10.1002/2015JB012519.

Duffy, O. B., R. E. Bell, C. A. L. Jackson,, R. L. Gawthorpe, and P. S. Whipp (2015), Fault growth and interactions in a multiphase rift fault network: the Horda Platform, Norwegian North Sea, *J. Struct. Geol.*, 80, 99–119, doi:10.1016/j.jsg.2015.08.015.

Elter, P., G. Giglia, M. Tongiorgi, and L. Trevisan (1975), Tensional and compressional areas in the recent (Tortonian to present) evolution of the Northern Apennines, *B. Geofis. Teor. Appl.*, 65, 3–18.

Finetti, I. R., F. Calamita, U. Crescenti, A. Del Ben, E. Forlin, M. Pipan, G. Rusciadelli, and V. Scisciani (2005), Crustal Geological Section across Central Italy from the Corsica Basin to the Adriatic Sea based on Geological and CROP Seismic Data, in *CROP PROJECT: Deep Seismic Exploration of the Central Mediterranean and Italy*, edited by I. R. Finetti, pp. 159–197, Elsevier.

Galadini, F., and P. Galli (2000), Active tectonics in the Central Apennines (Italy) – input data for seismic hazard assessment, *Nat. Hazards*, 22, 225–270; doi:10.1023/A:1008149531980.

Galadini, F., and P. Galli (2003), Paleoseismology of silent faults in the Central Apennines (Italy): the Mt. Vettore and Laga Mts. faults, *Ann. Geophys.*, 46(5), 815–836, doi:10.4401/ag-3457.

Galadini, F., and P. Messina (2001), Plio-Quaternary changes of the normal fault architecture in the Central Apennines (Italy), *Geodinamica Acta*, 14, 321–344, doi:10.1016/S0985-3111(01)01076-2.

Gallovič, F., and J. Zahradník (2012), Complexity of the Mw 6.3 2009 L'Aquila (Central Italy) earthquake: 1. Multiple finite-extent source inversion, *J. Geophys. Res.*, 117, B04307, doi:10.1029/2011JB008709.

Gallovič, F., W. Imperatori, P. M. Mai (2015), Effects of three-dimensional crustal structure and smoothing constraint on earthquake slip inversions: case study of the Mw6.3 2009 L'Aquila earthquake, *J. Geophys. Res.*, 120(1), 428–449, doi:10.1002/2014JB011650.

Ghisetti, F., and L. Vezzani (1999), Depth and modes of Pliocene-Pleistocene crustal extension of the Apennine (Italy), *Terra Nova*, 11, 67-72, doi:10.1046/j.1365-3121.1999.00227.x.

Kennett, B. L. N., and N. J. Kerry (1979), Seismic waves in a stratified half space, *Geophys. J. Int.*, 57(3), 557–583, doi:10.1111/j.1365-246X.1979.tb06779.x.

King, G., and J. Nabelek (1985), Role of fault bends in the initiation and termination of earthquake rupture, *Science*, 228(4702), 984–987.

Lavecchia, G., F. Brozzetti, M. Barchi, M. Menichetti, and J. V. A. Keller (1994), Seismotectonic zoning in east-central Italy deduced from an analysis of the Neogene to present deformations and related stress fields, *Geol. Soc. Am. Bull.*, 106(9), 1107–1120, doi:10.1130/0016-7606(1994)106<1107:SZIECI>2.3.CO;2.

Lavecchia, G., R. Castaldo, R. de Nardis, V. De Novellis, F. Ferrarini, S. Pepe, F. Brozzetti, G. Solaro, D. Cirillo, M. Bonano, P. Boncio, F. Casu, C. De Luca, R. Lanari, M. Manunta, M. Manzo, A. Pepe, I. Zinno, and P. Tizzani (2016), Ground deformation and source geometry of the 24 August 2016 Amatrice earthquake (Central Italy) investigated through analytical and numerical modeling of DInSAR measurements and structural-geological data, *Geophys. Res. Lett.*, 43(24), 12,389–12,398, doi:10.1002/2016GL071723.

Lawson, C. L., and R. J. Hanson (1974), *Solving Least Square Problems*, Prentice- Hall, Englewood Cliffs, N. J.

Livio, F., A. M. Michetti, E. Vittori, L. Gregory, L. Wedmore, L. Piccardi, E. Tondi, G. Roberts, and Central Italy Earthquake Working Group (2016), Surface faulting during the August 24, 2016, Central Italy earthquake (Mw 6.0): preliminary results, *Ann. Geophys.*, 59(5), doi:10.4401/ag-7197.

Luzi, L., R. Puglia, E. Russo, and ORFEUS WG5 (2016a), Engineering Strong Motion Database, version 1.0, Istituto Nazionale di Geofisica e Vulcanologia, Observatories & Research Facilities for European Seismology, doi:10.13127/ESM.

Luzi, L., R. Puglia, E. Russo, M. D'Amico, C. Felicetta, F. Pacor, G. Lanzano, U. Çeken, J. Clinton, G. Costa, L. Duni, E. Farzanegan, P. Gueguen, C. Ionescu, I. Kalogeras, H. Özener, D. Pesaresi, R. Sleeman, A. Strollo, and M. Zaré (2016b), The Engineering Strong- Motion Database: A Platform to Access Pan- European Accelerometric Data, *Seismol. Res. Lett.*, 87(4), 987–997, doi:10.1785/0220150278.

Manighetti, I., C. Caulet, D. De Barros, C. Perrin, F. Cappa, and Y. Gaudemer (2015), Generic along-strike segmentation of Afar normal faults, East Africa: Implications on fault growth and stress heterogeneity on seismogenic fault planes, *Geochem. Geophys. Geosyst*., 16, 443–467, doi:10.1002/2014GC005691.

Mildon, Z.K., G.P. Roberts, J.P. Faure Walker, and F. Iezzi (2017), Coulomb stress transfer and fault interaction over millenia on non-popular active normal faults: the Mw 6.5-5.0 seismic sequence of 2016-2017, central Italy, *Geophys. J. Int*., 210, (2), 1206–1218, doi:10.1093/gji/ggx213.

Patacca, E., and P. Scandone (2007), Geology of the Southern Apennines, *Boll. Soc. Geol. It.*, spec. vol. 7, 75–119.

Peacock, D. C. P., and D. J. Sanderson (1994), Geometry and development of relay ramps in normal fault systems, *American Association of Petroleum Geologists Bulletin*, 78, 147–165.

Peacock, D. C. P., C. W. Nixon, A. Rotevatn, D. J. Sanderson, and L. F. Zuluaga (2017), Interacting faults, *J. Struct. Geol.*, 97, 1–22, doi:10.1016/j.jsg.2017.02.008.

Perrin, C., I. Manighetti, J.-P. Ampuero, F. Cappa, and Y. Gaudemer (2016), Location of largest earthquake slip and fast rupture controlled by along-strike change in fault structural maturity due to fault growth, *J. Geophys. Res. Solid Earth*, 121, 3666–3685, doi:10.1002/2015JB012671.

Pierantoni, P. P., G. Deiana, and S. Galdenzi (2013), Stratigraphic and structural features of the Sibillini Mountains (Umbria-Marche Apennines, Italy), *Ital. J. Geosci. (Boll. Soc. Geol. It.)*, 132(3), 497–520.

Pizzi, A., and F. Galadini (2009), Pre-existing cross-structures and active fault segmentation in the northern-central Apennines (Italy), *Tectonophysics*, 476, 304–319, doi:10.1016/j.tecto.2009.03.018.

Pizzi, A., and V. Scisciani (2000), Methods for determining the Pleistocene-Holocene component of displacement on active faults reactivating pre-Quaternary structures: Examples from the Central Apennines (Italy), *J. Geodyn.*, 29, 3-5, 445–457.

Pizzi, A., F. Calamita, M. Coltorti, and P. Pieruccini (2002), Quaternary normal faults, intramontane basins and seismicity in the Umbria-Marche-Abruzzi Apennine Ridge (Italy): Contribution of neotectonic analysis to seismic hazard assessment, *Ital. J. Geosci. (Boll. Soc. Geol. It.)*, 1(2), 923–929.

Pondrelli, S., A. Morelli, G. Ekström, S. Mazza, E. Boschi, and A. M. Dziewonski (2002), European-Mediterranean regional centroid-moment tensors: 1997-2000, *Phys. Earth Planet. Int.*, 130, 71–101, doi:10.1016/S0031-9201(01)00312-0.

Pondrelli, S., S. Salimbeni, A. Morelli, G. Ekström, L. Postpischl, G. Vannucci, and E. Boschi (2011), European-Mediterranean Regional Centroid Moment Tensor Catalog: solutions for 2005-2008, *Phys. Earth Planet. Int.*, 185(3), 74–81, doi:10.1016/j.pepi.2011.01.007.

Pucci, S. et al. (EMERGEO W.G.) (2016), Coseismic effects of the 2016 Amatrice seismic sequence: first geological results, *Ann. Geophys.*, 59, 5, doi:10.4401/ag-7195.

Roberts, G.P., and A.M. Michetti (2004), Spatial and temporal variations in growth rates along active normal fault systems: an example from The Lazio – Abruzzo Apennines, central Italy, *J. Struct. Geol.*, 26, 339-376, doi:10.1016/S0191-8141(03)00103-2.

Rovida, A., R., Camassi, P., Gasperini and M., Stucchi (2011): CPTI11, the 2011 version of the Parametric Catalogue of Italian Earthquakes, Istituto Nazionale di Geofisica e Vulcanologia, Milano, Bologna, doi:10.6092/INGV.IT-CPTI11, 2011.

Scholz, C. (2010), Large Earthquake Triggering, Clustering, and the Synchronization of Faults, *Bull. Seismol. Soc. Am.*, 100(3), 901–909, doi:10.1785/0120090309.

Scholz, C.H., and A. Gupta (2000), Fault interactions and seismic hazard, *J. Geodyn.*, 29, 459–467.

Schwartz, D.P. (1989), Paleoseismicity, persistence of segments, and temporal clustering of large earthquakes—Examples from the San Andreas, Wasatch, and Lost River fault zones, U.S. Geol. Surv. Open File Rep. 89–315, 361–375.

Schwartz, D.P., and K.J. Coppersmith (1984), Fault behavior and characteristic earthquakes: Examples from the Wasatch and San Andreas fault zones, *J. Geophys. Res.*, 89, 5681–5698.

Scisciani, V., E. Tavarnelli, and F. Calamita (2002), The interaction of extensional and contractional deformations in the outer zones of the Central Apennines, Italy, *J. Struct. Geol.*, 24, 1647–1658, doi:10.1016/S0191-8141(01)00164-X.

Scisciani, V., S. Agostini, F. Calamita, P. Pace, A. Cilli, I. Giori, and W. Paltrinieri (2014), Positive inversion tectonics in foreland fold-and-thrust belts: A reappraisal of the Umbria–Marche Northern Apennines (Central Italy) by integrating geological and geophysical data, *Tectonophysics*, 637, 218–237, doi:10.1016/j.tecto.2014.10.010.

Servizio Geologico d'Italia (1941), *Carta Geologica d'Italia, scale 1:100.000, Sheet 132 "Norcia"*, Ist. Poligrafico e Zecca dello Stato, Roma.

Sibson, R.H. (1986), Rupture interaction with fault jogs, *Earthquake Source Mech.*, 37, 157–167.

Sokos, E., J. Zahradník, F. Gallovič, A. Serpetsidaki, V. Plicka, and A. Kiratzi (2016), Asperity break after 12 years: The Mw6.4 2015 Lefkada (Greece) earthquake, *Geophys. Res. Lett.*, 43, 6137-6145.

Susong, D.D., S.U. Janecke, and R.L. Bruhn (1990), Structure of a fault segment boundary in the Lost River fault zone, Idaho, and possible effect on the 1983 Borah Peak earthquake rupture, *Bull. Seismol. Soc. Am.*, 80(1), 57–68.

Tavarnelli, E., R. W.H. Butler, E.A. Decandia, F. Calamita, M. Grasso, W. Alvarez, and P. Renda (2004), Implications of fault reactivation and structural inheritance in the Cenozoic tectonic evolution of Italy in *Geology of Italy: Special Volume of the Italian Geological Society for the IGC 32 Florence-2004*, edited by U. Crescenti et al., pp. 209–222, Soc. Geol. It., Florence, Italy.

Tinti, E., L. Scognamiglio, A. Michelini, and M. Cocco (2016), Slip heterogeneity and directivity of the ML 6.0, 2016, Amatrice earthquake estimated with rapid finite-fault inversion, *Geophys. Res. Lett.*, 43(20), 10,745–10,752, doi:10.1002/2016GL071263.

Wells, D.L., and K.J. Coppersmith (1994), New empirical relationships among magnitude, rupture length, rupture width, rupture area, and surface displacement, *B. Seismol. Soc. Am.*, 84, 974–1002.

Wesnousky, S.G. (2008), Displacement and geometrical characteristics of earthquake surface ruptures – Issues and implications for seismic-hazard analysis and the process of earthquake rupture, *Bull. Seismol. Soc. Am.*, 98(4), 1609–1632, doi:10.1785/0120070111.

Table 1. Magnitude and location of the three main events of the 2016 Central Italy sequence (* from http://cnt.rm.ingv.it; § from *Chiaraluce et al.* [2017]).

Lon§	Lat§	Depth§ (km)	Mw*	Date and time
13.251	42.704	7.93	6.0	2016-08-24 01:36:32
13.088	42.904	4.45	5.9	2016-10-26 19:18:05
13.121	42.835	7.32	6.5	2016-10-30 06:40:17

Table 2. Results of the finite fault inversion (*refers to location of the centroid calculated from the inverted slip distribution).

Rake	Dip	Strike	Lon*	Lat*	Depth*	Mw	Date and time
-85	45	155	13.24	42.73	4.7	6.2	2016-08-24 01:36:32
-80	40	160	13.12	42.94	4.2	6.1	2016-10-26 19:18:05
-90	40	160	13.19	42.80	3.8	6.5	2016-10-30 06:40:17

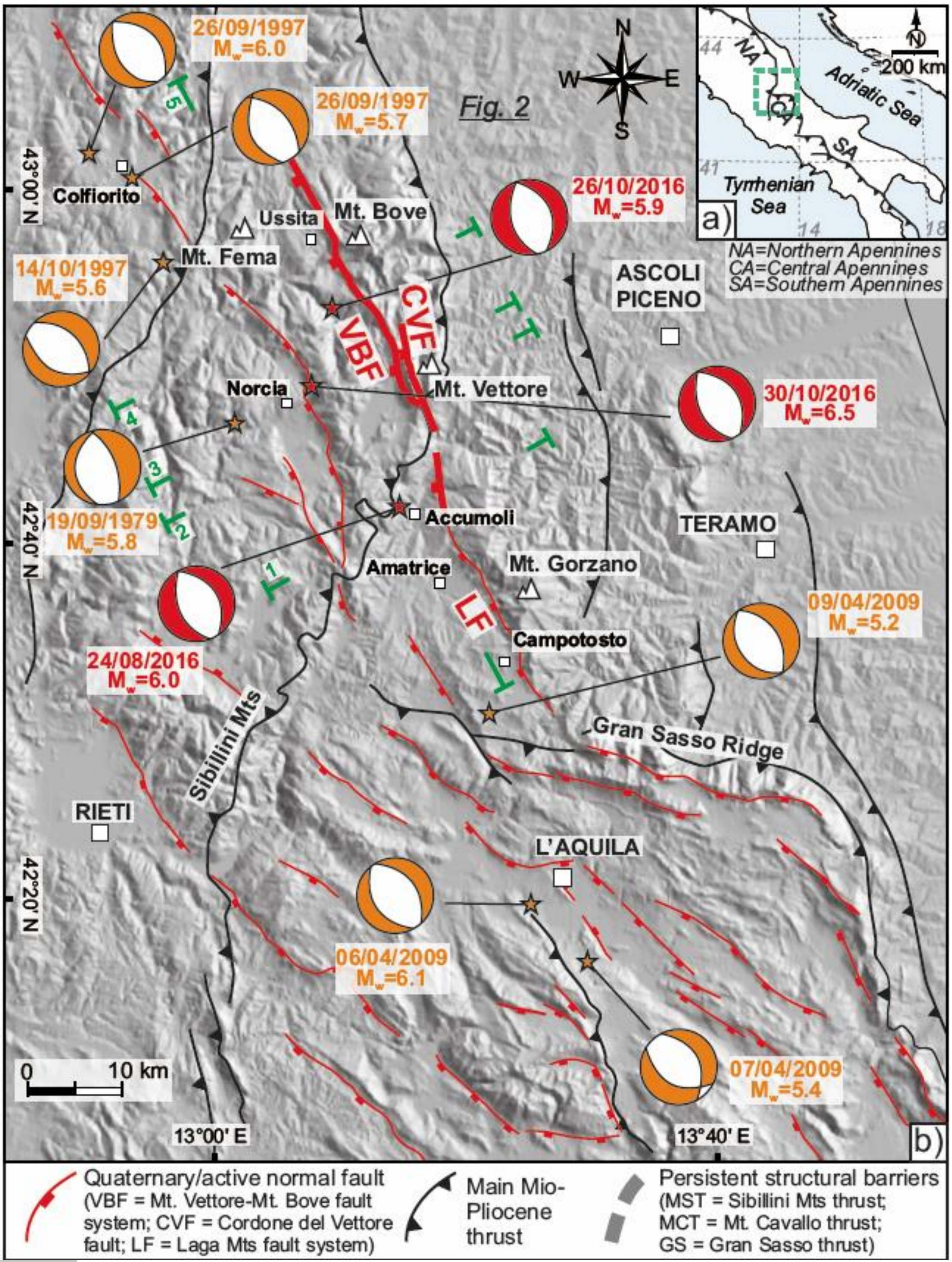

Figure 1. a) Location map of Figure 1b with the three main arcs of the Apennine chain. b) Seismotectonic sketch of the study area with the main thrusts (black lines) and Quaternary/active normal fault systems (red lines). Thick red lines indicate the normal faults involved in the 2016 seismic sequence. Focal mechanisms of the 2016 (in red) and other main recent seismic sequences are reported. The Mt. Cavallo (MCT), Sibillini Mts (MST) and Gran Sasso (GS) thrust ramps are oblique to the main (N)NW–(S)SE trend of the normal fault systems. In green: traces of the cross-sections shown in Figures 6 and 7.

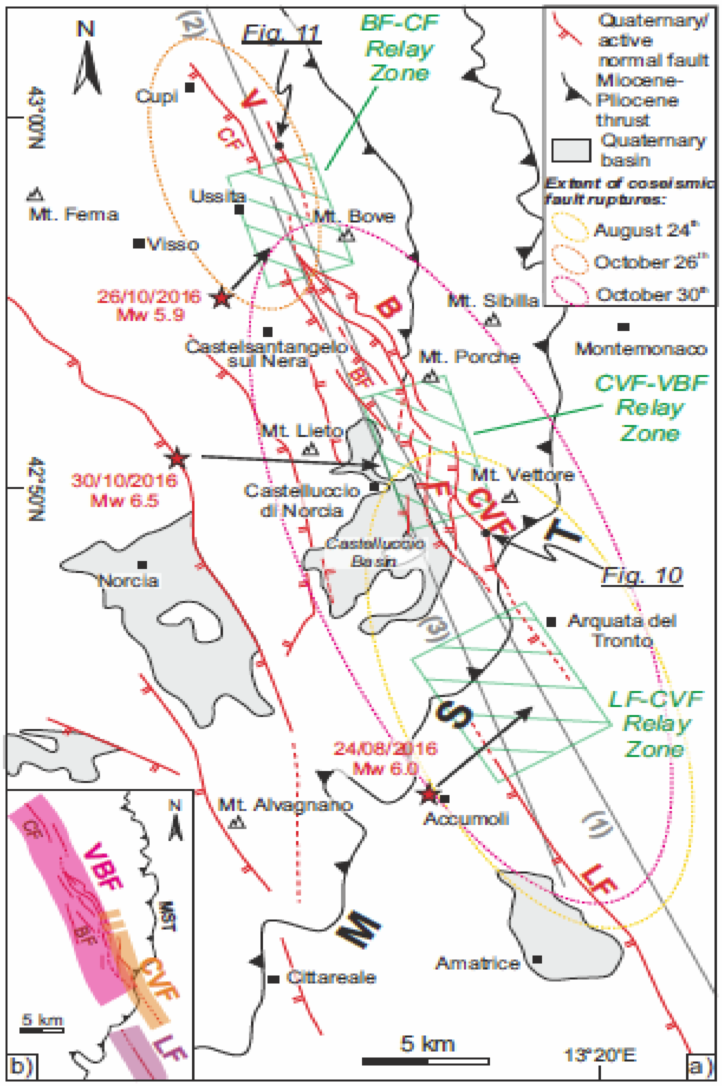

Figure 2. a) Simplified structural map of the area struck by the 2016 Central Italy seismic sequence (see Figure 1 for the location) in which the Quaternary/active normal faults (from *Calamita et al.* [1992], except the west-dipping fault affecting the Castelluccio basin, that is from *Galadini and Galli* [2003]), the main Miocene-Pliocene thrust planes (MST: Sibillini Mts thrust) and the extent of observed coseismic surface ruptures are reported. The projections of the fault planes considered in the slip inversion for the three main events and showed in Figures 3 and 4 are reported (grey thick lines: 1 - Amatrice event; 2 - Ussita event; 3 - Norcia event). The Mt. Vettore–Mt. Bove normal fault system (VBF) is composed of several normal fault segments among which we distinguish the northernmost Cupi segment (CF), probably activated during the October 26th Ussita event, from the central–southern sector (BF: Mt. Bove segment) (b). The Cordone del Vettore fault (CVF) runs along the Mt. Vettore western slope and displaces the MST at surface. The Laga Mts fault system (LF) affects the MST footwall block. Polygons with green oblique lines indicate relay zones between adjacent normal faults where the three main shocks probably nucleated. Dotted ellipses represent the extent of observed ground ruptures along the VBF and CVF fault systems (this study) and LF (after *Pucci et al.*, [2016]) for each of the three major events.

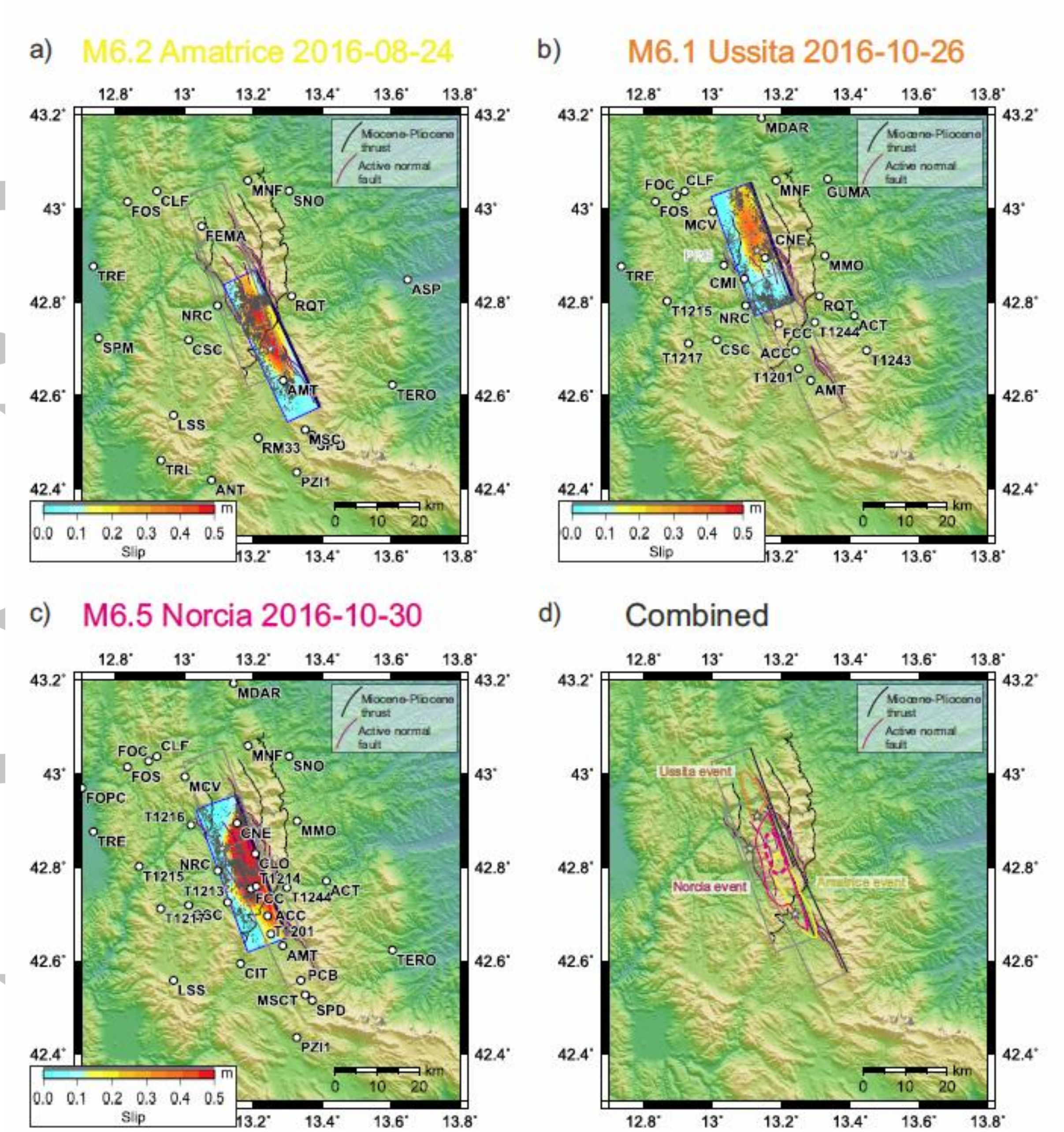

Figure 3. a) Slip distribution of the Amatrice event projected on the surface with corresponding fault (blue rectangle), epicenter (stars) and stations used in the inversion (circles). On-fault aftershocks of the whole sequence [*Chiaraluce et al.*, 2017] are plotted by grey dots. Grey rectangles correspond to the other faults shown for easier visual comparison. b) Same as (a) but for the Ussita earthquake. c) Same as (a) but for the Norcia earthquake (note the saturated color scale; the maximum slip reached is 3 m). d) Combined plot of the contour of 0.3 m slip (thin lines) for all the three events and of 1.5 m for the Norcia event (thick dashed line). For the location of the fault top edges see also Figure 2.

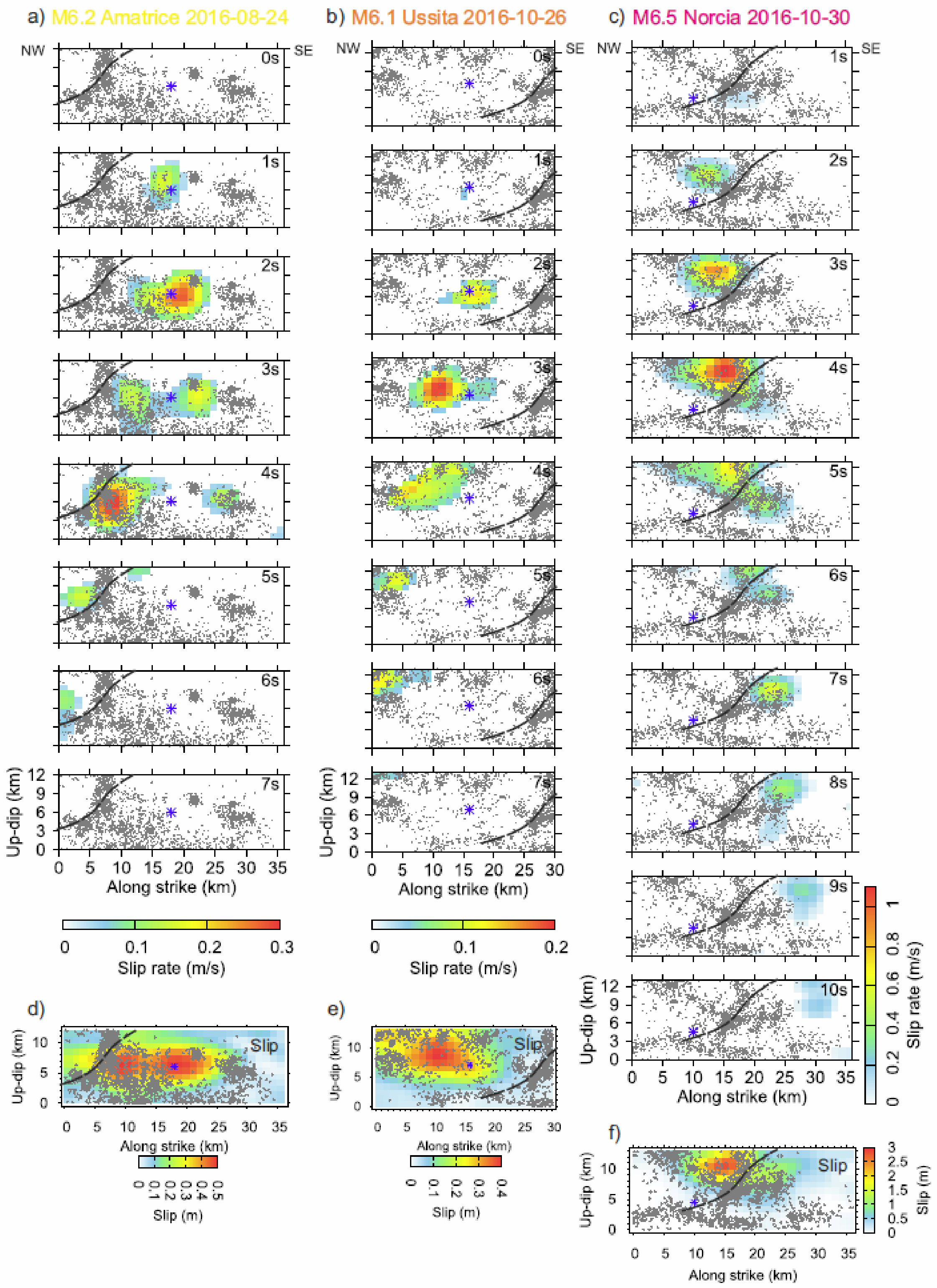

Figure 4. Slip rate snapshots showing rupture evolution in time for the three analyzed events. The points represent on-fault aftershocks of the whole sequence. Color scales are different to highlight individual slips on faults (*i.e.*, events located within 0.5 km from the model fault plane). We have omitted the snapshot at 0s for the Norcia event as the slip rate was negligible along the fault. The black dashed line sketches the fault intersection with MST. See Figure 2 for the location of the fault top traces.

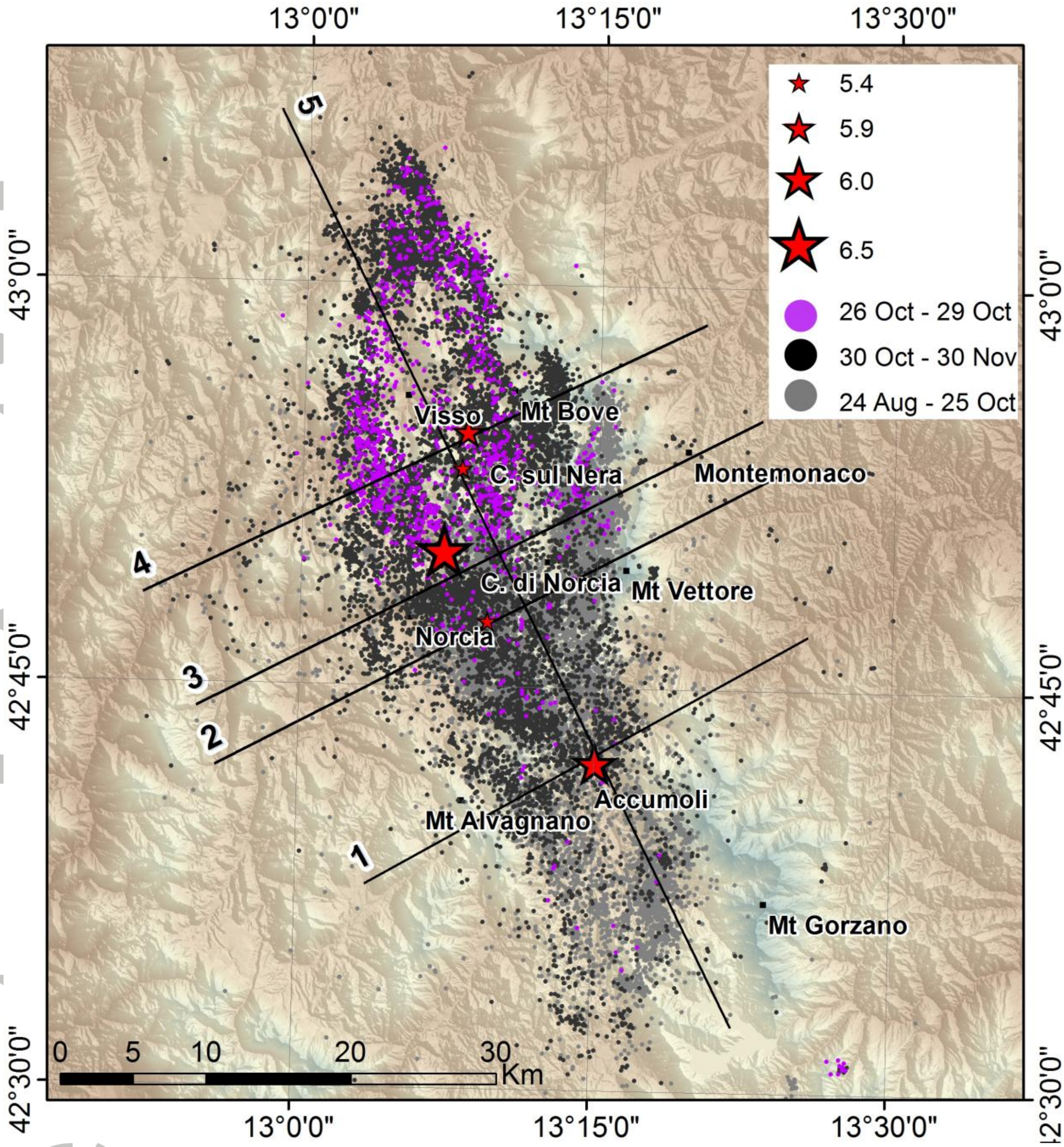

Figure 5. Location of the five events with magnitude larger than 5 (red stars) and aftershocks distribution from *Chiaraluce et al.* [2017] (dots are colored according to different time periods). Black lines are the cross-sections shown in Figures 6 and 7.

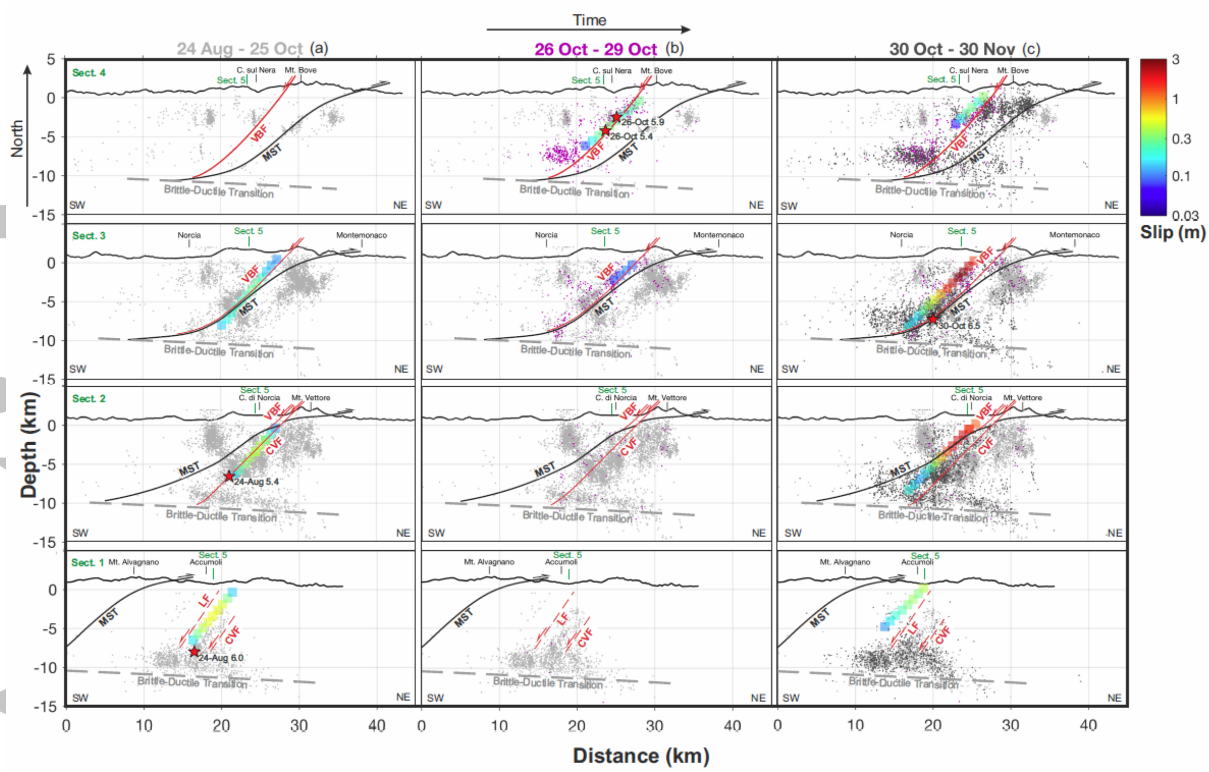

Figure 6. Cross-sections 1-4 (traces in Figures 1 and 5) showing the main events, the aftershocks and the fault slip (transposed on the cross-section vertical plane) for each period. Geometric relationships between the MST (black line) and the normal faults involved during the 2016 seismic sequence (red line or red dashed line if the prosecution of the fault is supposed at depth) are displayed. Grey dots are aftershocks in the period 24/08–25/10, purple dots are aftershocks in the period 26/10–29/10 and black dots are aftershocks in the period 30/10–30/11. Looking at the evolution of the sequence both in time (from August 24th to October 30th) and space (from section 4, to the north, to section 1, to the south) the activated normal faults and their relationships with the MST barrier are visible. In column “c” the misfit between the projection of the slip and fault geometry may be due to the simplification of the slip model and/or to the uncertain geometry of faults at depth.

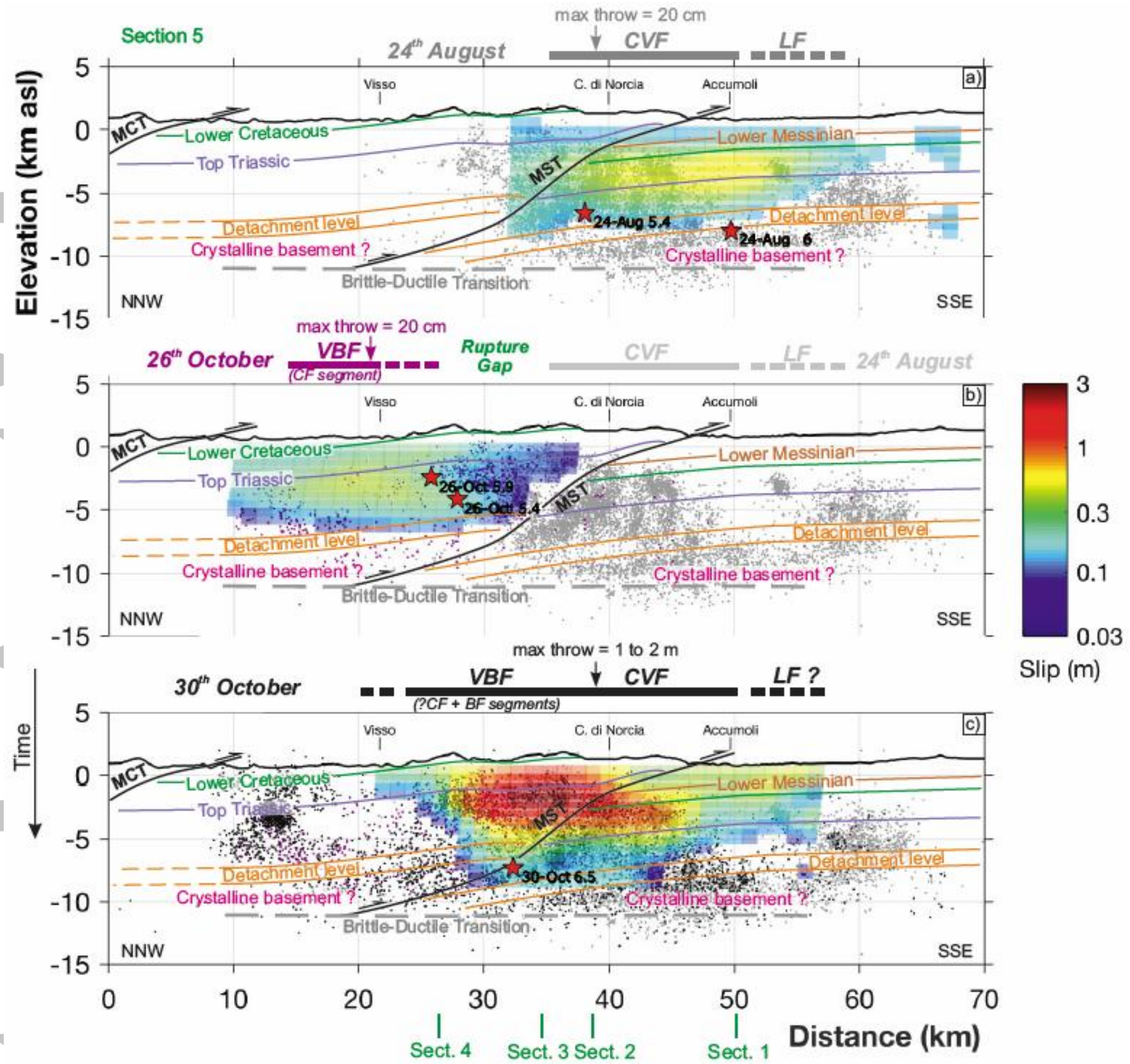

Figure 7. Cross-section parallel to the faults strike (trace 5 in Figures 1 and 5) comparing rupture length and slip amount from inversion method with field observations: thick lines above each profile and thick dashed lines, where uncertain, indicate rupture length observed at surface; arrow indicates the site where the maximum surface throw was observed (surface rupture length along the Laga Fault are from *Pucci et al.* [2016]). Note the good correspondence between the two dataset regarding ruptures extent and zones of maximum slip. On the cross-section the locations of the main events, fault slips from inversion analysis (transposed on the cross-section vertical plane), aftershocks distribution (grey dots are aftershocks in the period 24/08–25/10, purple dots are aftershocks in the period 26/10–29/10 and dark gray dots are aftershocks in the period 30/10–30/11), the main geological boundaries and the MST are represented. The MST controlled the propagation and distribution of slip and seismicity, confining the ruptures of August 24th and October 30th. The October 30th nucleated in correspondence of the MST and the associated slip involved the area remained almost unruptured after the first two main shocks. See text for further explanations.

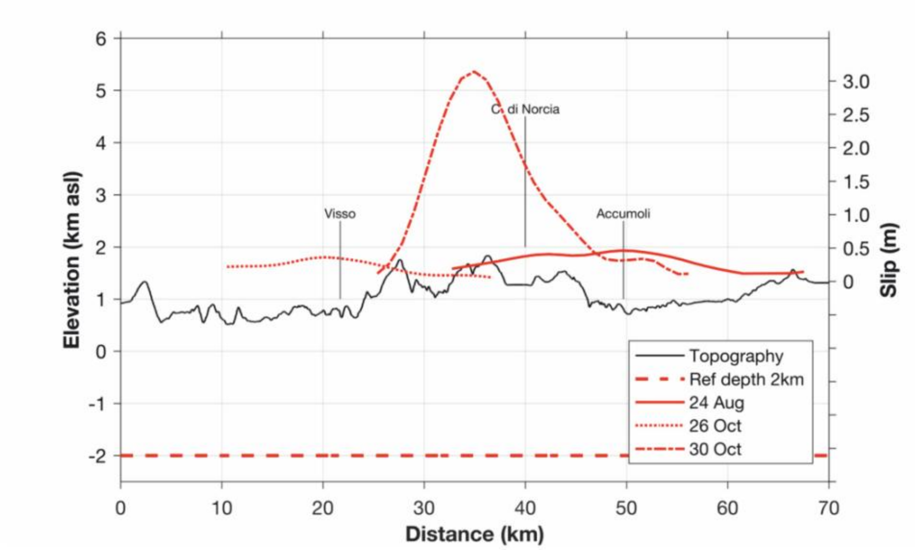

Figure 8. Slip distribution along section 5, at a reference depth of 2 km. After the first two events the central sector of the area is characterized by a slip gap, that corresponds to the largest slip of the strong-motion inversion (October 30th event).

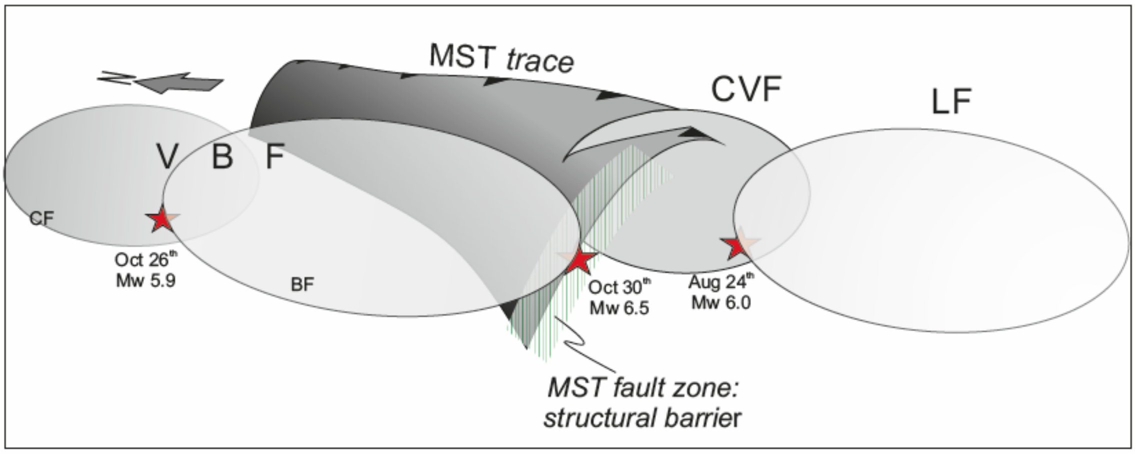

Figure 9. Schematic 3D model of the 2016 Central Italy earthquakes rupture zones, not to scale. Red stars are the three main shocks; ellipses represent the active normal faults (LF: Laga Mts normal fault; CVF: Cordone del Vettore normal fault; VBF: Mt. Vettore–Mt. Bove normal fault system with the BF: Mt. Bove and CF: Cupi fault segments); MST: Sibillini Mts pre-existing oblique thrust ramp acting as a structural barrier. Only the shallower low-angle part of the MST is displaced by the CVF, which ruptured up to surface. The MST high-angle fault zone, instead, still likely represents a structural barrier at depth, limiting the rupture of August 24th and, probably, October 26th and concentrating the local stress until the rupture of October 30th nucleated on it. The fact that the Mw 6.5 event activated both the VBF and CVF, however, suggests that, at least, there is a kinematic soft-linkage at the relay zone between these two faults and even that the CVF has probably started to breach through the fault zone of the MST barrier. The August 24th and October 26th ruptures initiated at the relay zones between LF and CVF and between BF and CF, respectively.

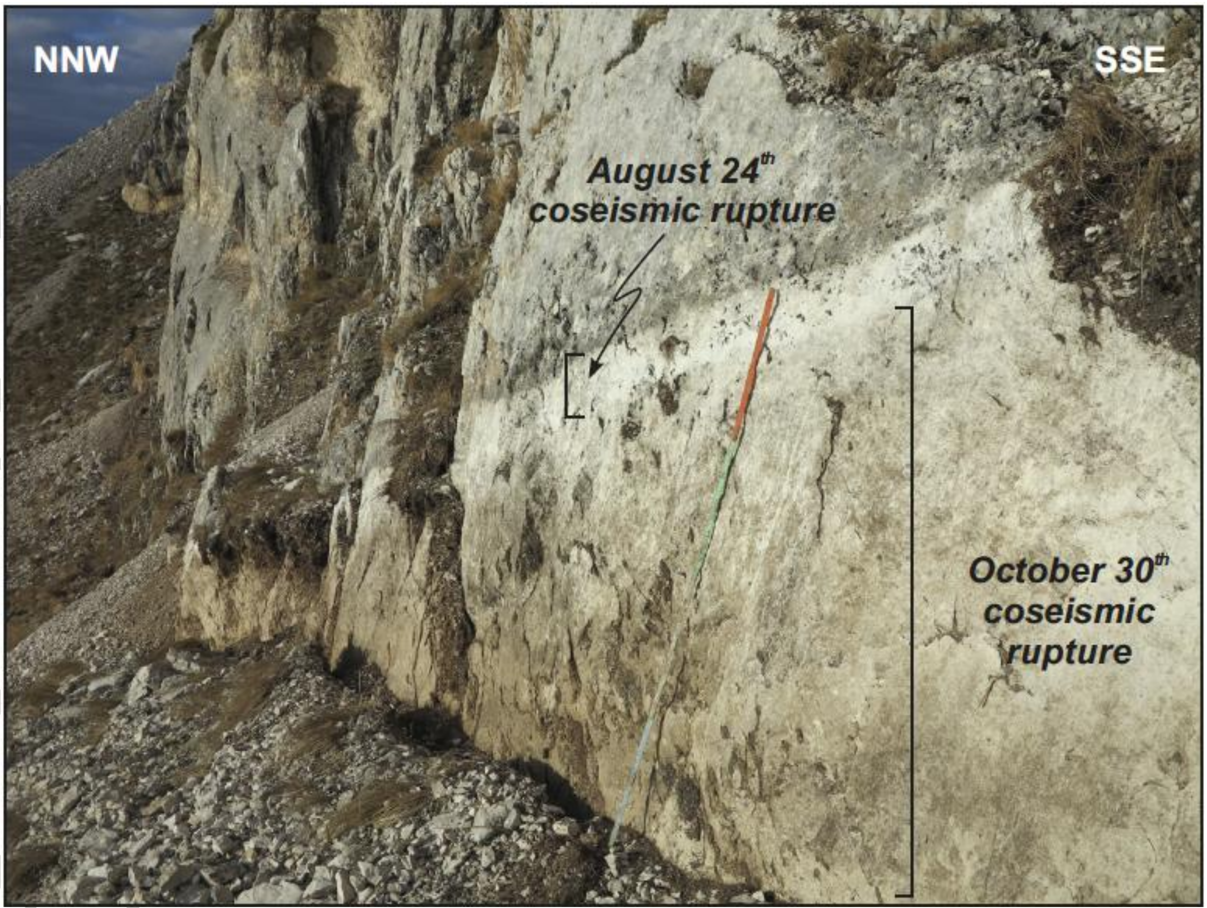

Figure 10. Coseismic surface ruptures occurred along the Cordone del Vettore fault (see Figure 2 for the location). This fault has been activated by both the Amatrice event, recording ca. 20 cm of coseismic slip, and the Norcia one, after which the fault showed the maximum surface rupture (1 to 2 meters) of the entire area. The two ruptures are recognizable as they are represented by two lighter bands of unweathered (*e.g.*, not previously exposed) limestone at the base of the fault plane. The August 24^{th} throw appears as the brightest band because it was cleaned by the September-October rains, while the October 30^{th} is still smeared by the faulted soil dragged along the fault plane (picture taken on December 3^{rd}, 2016).

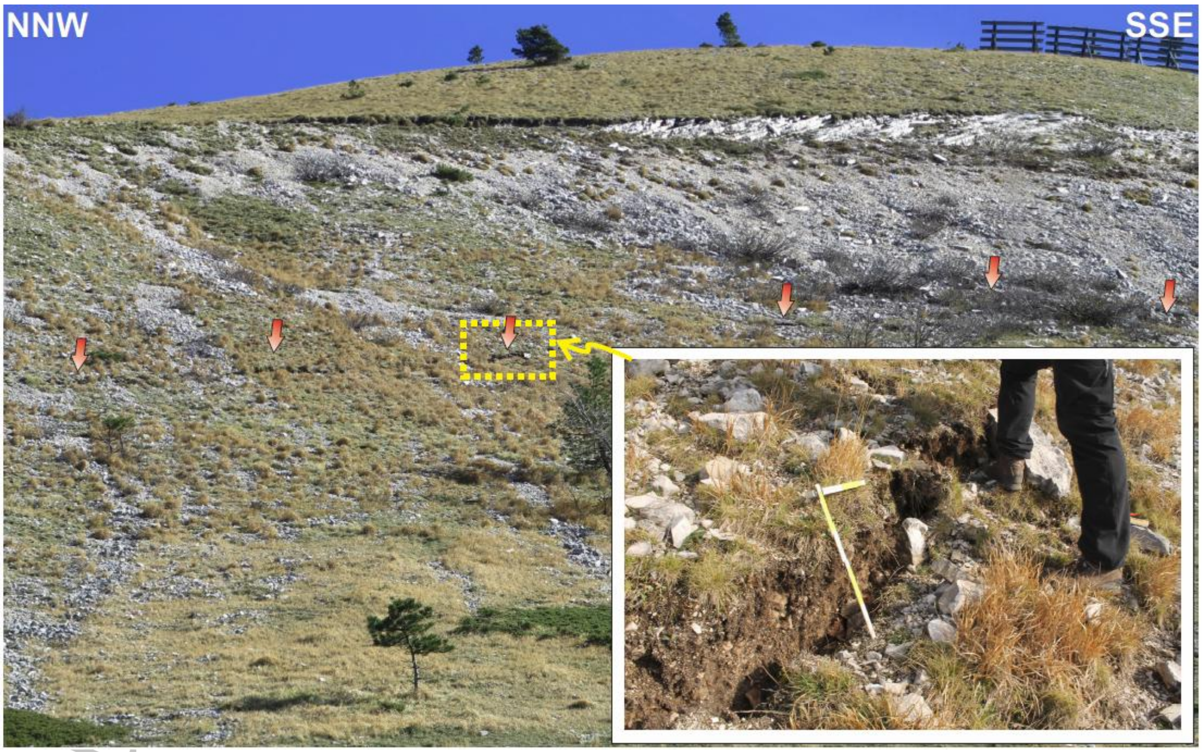

Figure 11. Coseismic surface ruptures occurred along the Casali fault (see Figure 2 for the location). This fault has been activated during the Ussita event, recording a maximum coseismic slip of about 20 cm (picture taken on October 27th, 2016).

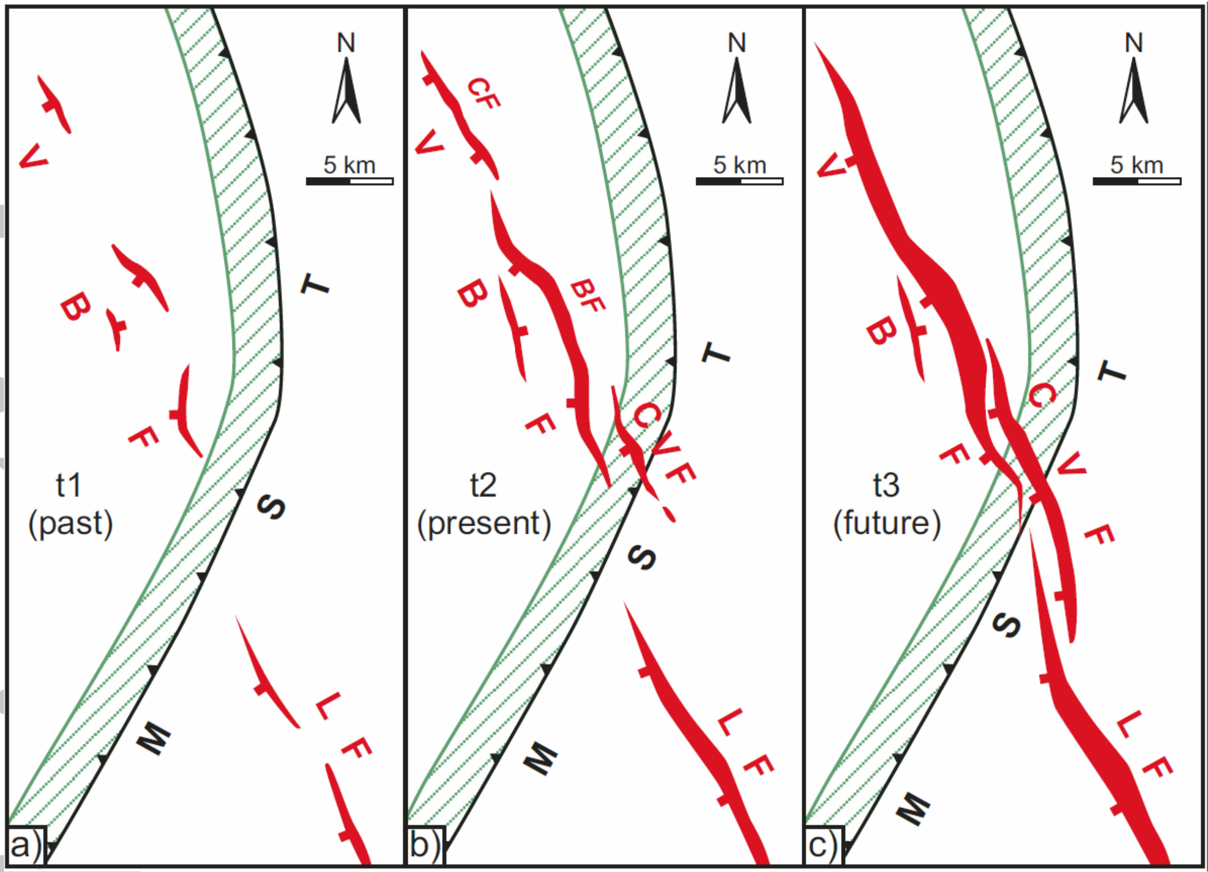

Figure 12. Schematic evolution of the normal fault systems affecting the study area. Fault segments have grown independently, separated by MST (a) VBF (CF+BF) and LF become kilometers-long fault systems and CVF starts developing as a distinct fault displacing the MST (b). This stage may represent the present-day setting where CVF is working as a soft-linkage structure between VBF and CVF and has to recover the displacement gap growing faster than the adjacent faults. Probably in the future, MST could be by-pass through the hard-linkage of VBF, CVF and LF (c).